POLITECNICO DI TORINO

Master's Degree in Mechatronic Engineering

Master's Degree Thesis

Design and implementation of a torque vectoring control for Formula Student Driverless application

Supervisors

Prof. Nicola AMATI

PhD Raffaele MANCA

Candidate

Alessandra DI GENNARO

July 2024

To my beloved family
and
to my closest friends.

Abstract

This thesis work is focused on the design of a Torque Vectoring (TV) architecture for a 4WD (Four Wheel Drive) electrical racing, in the context of the participation by the Polytechnic of Turin in the Formula Student Driverless competition organized by the Society of Automotive Engineers (SAE).
The TV aims to optimally distribute the total required torque, both in traction and in braking, in order to produce an additional moment acting on the vehicle's yaw rate. The control TV architecture is mainly composed of three subsystems: a Reference Generator, a High-Level Controller based on a Linear Quadratic Regulator (LQR) and a Low-Level Controller for the motor torque allocation to the wheels, solving a Quadratic Programming (QP) optimization problem.
This project is based on a co-simulation between Vi-CarRealTime and MATLAB/Simulink. The former provides an accurate full Degree of Freedom model of the vehicle and represent the plant of the whole control system; the latter, instead, is actually used for the development of the Torque Vectoring controller and the simulation set up.
Due to the autonomous feature of the prototype, the simulations have been conducted generating a pre-planned path by MATLAB script and employing a Model Predictive Controller (MPC) for guaranteeing the path tracking.
The developed Torque Vectoring aims to control the lateral dynamics of the prototype to enhance its cornering performances by the allocation of a suitable torque to each in-wheel electric motor. A remarkable consideration highlighted by the results is the advantage of the TV regarding the MPC, since the TV acts as a model following to force the plant model to work more accurately and closer to the predictive model, preventing model mismatches due to non-linearities, approximations and eventual inexact parameters estimations.

Table of Contents

1 Introduction

1.1 Thesis objectives

The constant innovations in automotive have highlighted a particular concentration towards new control strategies to enhance the vehicle's safety and performances, especially by the introduction of the autonomous cars.

This thesis is focused on the design of a Torque Vectoring (TV) architecture to control the lateral dynamics of an autonomous all-wheel-driving (AWD) electrical vehicle prototype by an optimal distribution of the torque on the four wheels. For the participation of Polytechnic of Turin in the Formula Student competitions, the aim is to demonstrate the benefits coming from the integration of TV in the low-level controller of the prototype, with a particular focusing on the improvements achieved in the path tracking performed by the already integrated Model Predictive Control (MPC).

1.2 Torque Vectoring (TV)

The incoming of the electric vehicles over the years has introduced relevant improvements in the automotive industry, from the energy efficiency to the vehicle handling and stability. The most promising approach in terms of efficiency and improving of the vehicle dynamics is the introduction of in-wheel electric motors, one embedded in each motor shell. Moreover, the possibility to individually control the torques exerted by the four electric motors has allowed the development of new control strategies enhancing the vehicle manoeuvrability and dynamic performances.

Particularly, the Torque Vectoring (also called Direct Yaw Moment Control) consists of the dynamically allocation of the torque by piloting each in-wheel motor, enabling the control of the vehicle yaw rate and then the increasing of the

vehicle stability in limit conditions. In fact, the generation of an additional yaw moment gives the opportunity to increase the lateral dynamics of the vehicle, obtaining a higher yaw rate at the same steering input value, without exceeding in slipping conditions.

The human-driven vehicles have largely integrated Torque Vectoring (TV) control, especially the ones which have available on-board electric motors due to their easier controllable feature than the combustion vehicles. However, the most common cases, which have also the most promising reachable performances, foresee the integration of TV in vehicles allowing a separate control of the each in-wheel powertrain due to the reliability and precision actuation of the electrical motors.

The results achieved up to now by the TV application are the improving of the vehicle's handling and cornering performances, meanwhile guaranteeing the driver's safety. [1], [2], [3], [4]

A common torque vectoring control architecture often employed in some publications foreseen a subdivision into three main sub-blocks respectively finalized to generate vehicle yaw rate and sideslip angle references to obtain a desired vehicle dynamics, a high-level controller for the generation of the yaw moment contribution and a low-level controller for the computation of the torque to be distributed to each motor wheel. [2], [3], [5]

Many studies in literature propose several types of controllers which not only regulate the yaw rate of the vehicle with respect a yaw rate reference, but that also aim to control a combination of vehicle yaw rate and vehicle side-slip angle for a more robust control system in every driving contest. The first state is particularly used to control the vehicle lateral dynamics, since its great influence on the vehicle handling. The vehicle side-slip angle, instead, is a relevant contribute for the monitoring of the vehicle's stability. However, the employment of the desired values of these two states as references can be sometimes challenging due to the contrast of the aimed results, as the increasing of the vehicle lateral dynamics and the improving of the vehicle's stability.

Additionally, the approaches described in literature generally present reference generator on the basis of the linear understeering gradient of a vehicle, feedforward strategies and even the selection of a driving mode. [1], [3]

Regarding the high-level controller, instead, the most common strategies developed concern the exploitation of Proportional-Integral (PI) and Proportional-Integral-Derivative (PID) controllers, which are very simple but effective for obtaining the desired traction/braking torque demand and the corrective moment to be generated to follow the references of the previous block. Other methods

include the implementation of Linear Quadratic Regulator (LQR), H-infinite and fuzzy logics controllers for the reaching of furtherly stabilized control system.[3] In the end the low-level control has the aim to allocate the suitable torque on each motor to satisfy the required torque and yaw moment, hence the most common strategies employ still fuzzy logic, Quadratic Programming (QP) control and Linear and Non-Linear Model Predictive Control (MPC), aiming to distribute the torque while minimizing the tires workload, power losses and increasing the tires adhesion and vehicle's stability and performances. [3]

1.2.1 Application of TV in autonomous vehicles

Concerning the autonomous driving application, the integration of advanced sensor technology to supersede any driver's operation has the aim to implement the main driverless functionalities of perception, path planning and path tracking. Regarding the last capability, several control strategies have been proposed with the scope of achieve the planned reference path for a successful vehicle's motion in an unknown environment. For the reaching of the path tracking task, optimal controllers are researched on the basis of Stanley Controller and Model Predictive Control (MPC), both linear and non-linear, according to the level of complexity chosen to be implemented. [6]

As already mentioned, nowadays the TV control is largely employed in the human-driven electrical vehicle, however its application for the driverless automotive is still in the beginning of its exploration. [4]

The solutions proposed in literature generally foreseen the application of a torque vectoring control to further guarantee the path tracking, i.e. by controller as MPCs, and maintain the vehicle stability preventing slipping conditions. [4], [7], [8]

In fact, the implementation of torque vectoring in the vehicle low-level controller acts trying to eliminate, or at least minimize, the error between the yaw rate measured and the yaw rate reference to achieve vehicle dynamics as close as possible to the predicted one. Especially in absence of the driver, this goal is essential for the validation of the estimations computed by the predictive controllers for a successful autonomous driving [4], [7]. The presence of model linearization and uncertainties can lead to a response different from the expected one; however, the integration of TV controller can influence the vehicle meas-

ured states to closely achieve the target yaw rate and side-slip and the traction/braking demand. Moreover, some studies describe the application of torque vectoring also in racing prototypes for the Formula SAE competition, with the aim of increasing the tires lateral forces for preventing slipping conditions and improving the vehicle handling. [4]
This thesis work presents the analysis and discussions concerning the application of a torque vectoring control to an autonomous racing prototype, alongside an already implemented MPC for the provision of the optimal steering angle.

1.3 Formula SAE

The Society of Automotive Engineers (SAE), officially known as SAE International, is a global association of engineering professionals with the aim of providing advancement and developing engineering standards in the fields of aerospace, automotive and commercial vehicle industries.
Founded in the 1905 for solving common technical problems in the field of automotive, currently the association can count more than 128'000 members. SAE annually shares the latest discoveries and technical information among the community through publications and magazines all over the world. [9]

Currently, the SAE is particularly oriented forward to the Advanced Driver Assistance Systems (ADAS) which are mainly focused on the enhancement of the vehicle safety and efficiency. In particular, ADAS rely on the employment of advanced technology sensors in other to detect the surrounding environment in real-time. In this way, the driver could be informed about eventual risks and he is able to intervene properly. In some cases of lacking of driver's action, the ADAS system can also actuate the opportune corrective action allowing to prevent critical situations.
Thanks to its leader role in the automotive field, SAE has influenced particularly the world of vehicles introducing the taxonomy J3016 which defines six levels of automation for vehicles. [10], [11]
In 2019, the SAE's Levels of Driving Automation has been adopted also by the National Highway Traffic Safety Administration (NHTSA) and it can be shortly summarized below [10]:

- Level 0, Momentary Driver Assistance. The human driver has the totally responsibility of driving, and all the vehicle features are assistive. [12]
- Level 1, Driver Assistance. The Advanced Driver Assistance (ADAS) provides continuous assistance in the vehicle driving, assisting in some case the human driver with either steering or accelerating/braking. [12]
- Level 2, Additional Assistance. In some circumstances, the ADAS provide assistance to the human driver, who still have the main control of driving, with both steering and accelerating/braking. [12]
- Level 3, Conditional Automation. The ADAS actively performs the vehicle driving, allowing the human driver to resume all the control when requested for necessary tasks. [12]
- Level 4, High Automation. The ADAS is responsible for the vehicle driving within some cases of limited-service areas in which the human driver attention is not required. [12]
- Level 5, Full Automation. The ADAS is totally responsible for the vehicle driving in ever circumstances. So, the human driver is considered as a passenger whose attention and its involving will not ever required. [12]

Examples of autonomous actions for the driver's support are the collistion avoidance systems, actuation of adaptive cruise control, lane keeping assist, emergency braking, automatic parking, pedestrian traffic signs recognition, and blind spot monitoring systems. [13]

One of the most challenging contests, committed by the SAE, is the Formula SAE (FSAE), occurred for the first time in the 1981. Formula SAE is a university competition which involves engineering students into the total developing of a racing car prototypes from the design of each mechanical, electronic components to the actual realization. This enables the members to deal with several features of the developing project not only concerning the technical details but also financial.
Starting with the internally combustion vehicle (CV) category, the Formula SAE has introduced through the years new categories as for the Hybrid Vehicles in 2007, Electric Vehicles (EV) in 2010 and recently the Driverless Vehicles (DV) in 2017, which aims to include the part of the ADAS capabilities explained above. Hence, this competition is a stimulant opportunity for research in the automotive field and experiment in practise the innovations just discovered, following the actual trends in the automotive field.

Entering in details, the Driverless competition foreseen an autonomous racing car dealing with a track circuit delimited by cones. Thanks to the sensors on board, the vehicle has to recognize the lanes of the track distinguishing the colours (yellow and blue) of the cones and their different shapes, without any driver guidance.
Typically, the competition is subdivided into a series of static and dynamic events. For what regards the static events, they can be summed up as below:

- Design event, in which the team has to present to the commission the engineering design followed, comprehensive of all the enhancements actuated concerning the overall prototype. This includes control strategies, electronics and mechanics of the car and so on.
- Cost event, which aims to evaluate the cost effort of the upgrades apported by the team in the season. This event aims to make the team's members an economical management conception of the manufacturing and industrial costs.
- Business plan event, in which the team has to present ideas for promoting the prototype advantages apported.

Instead, the dynamic events are:

- Acceleration, consisting in a vehicle's straight acceleration from resting position over 75 meters.
- Skidpad, consisting in track composed by two circles creating a shape of 8 circuit. The track has standard dimension delimited by cones and the vehicle has to perform twice each circle.
- Autocross, in which the vehicle deals with an unknown track with curves, straight pieces and chicanes. Hence, here the abilities of the prototype in recognizing the lanes perceptions are tested.
- Trackdrive, consisting in run 10 times the unknown track, aiming to evaluate the time for covering all the laps and, thus, the performances of the autonomous control strategy adopted.

1.4 Squadra Corse Driverless Team

1.4.1 The SCD Team

In the 2021 the Polytechnic of Turin founded the Squadra Corse Driverless (SCD) for the conduction of research in the autonomous driving field. Thanks to a collaboration with the Centre of Automotive Research and Sustainable mobility (CARS@PoliTO) and with the LIM laboratory of PoliTO, a disused racing prototype, from previous seasons of FSAE non-driverless competition, has been adapted for the autonomous driving. Mainly, an Autonomous Steering System and an Autonomous Braking System have been installed on the car. Then, it has been proceeded with the implementation of the fundamental autonomous capabilities of environment perception, path planning, state estimation, obtaining finally the first prototype of the Driverless Team.
The precedent season of 2023 has been focused in enhance the capabilities and performances of the car, by a redesign of the vehicle's hardware and software. Two stereo cameras and a LiDAR have been installed to improve the cone identification and positioning task, together with a reformulation of the data processing. For the path planning and path tracking, a SLAM algorithm, MPC and low-level control have been integrated too. A redesign of the battery pack and electronics have been conducted in parallel.
The introducing of these upgrades has guaranteed the increasing of the performances and reliability of the prototype.

1.4.2 The VaLentina Prototype

The prototype, called 'VaLentina' by the Team, is an all-wheel electric vehicle, with the electric motor integrated in the wheels. The maximum power and torque that they can exert are 35kW and 21Nm. By the presence of a gear transmission between the motor and the wheels, the maximum torque applicable to each wheel is 313Nm, considering the gear fixed velocity reduction value of 14.92.
It is possible to pilot each motor independently, controlling them by the inverters supplied by the owner manufactures, allowing the torque vectoring implementation.
As already explained, the presence of stereo-cameras and Lidar and the implementation of sensor fusion allow the identification in colour, shape and position of the cones delimiting the lane of the track.

Extended Kalman Filter manipulating and filtering the data coming from the sensors on the vehicle, have provided an optimized states estimation too.
The MPC has been integrated on the autonomous control unit (ACU), while the steering, braking and traction controls, including a torque vectoring strategy, compose the low-level control which has been implemented in the electronic control unit dSPACE MicroAutoBox III Real Time hardware.

Figure 1.1 – The VaLentina prototype

1.5 Thesis outline

First of all, in the following chapters an analysis of vehicle model is reported describing the first analytical part of this thesis research. This is a fundamental step in order to identify the suitable model to be employed according to the desired level of complexity and scope of this project.

A complete description of the controllers developed in this thesis follows in Chapter 3, with a particular focus on the Torque Vectoring Control strategy actuated together with a synthetic overview on a simplified Model Predictive Controller to simulate the controller already integrated on the prototype.

Finally, the simulation environment is explained and results obtained are presented and discussed, followed by the a conclusive briefing on the overall advantages derived by the application of the Torque Vectoring controller.

2 Vehicle Model

In order to properly design a control system, it is necessary to conduct an analysis focused on the dynamics of the system to be controlled. Hence, this chapter deals with the study of the vehicle model employed in this thesis project for the development of the controller in MATLAB/Simulink.
In particular, a mathematical approach is followed to represent the vehicle, that is essential for the understanding of the behaviour of the system and for the evaluation of the performance, limits and constraints.
There exist several vehicle models which allow to evaluate particular performances and parameters of the vehicle and, for this reason, which are more or less complex according to the case of study.

According to the Formula SAE regulations, the vehicle to be modelled is 4 Wheel Driving (4WD) electric prototype race car. The four vehicle's wheels are equipped with four in-wheel electric motors, coupled to the wheels thanks to a fixed transmission ratio.
For the developing of the Model Predictive Controller and the Torque Vectoring, the classic single track bicycle model with 3 Degrees of Freedom (DoF) is sufficient for the study of the vehicle's lateral dynamics.

2.1 Wheels and Tires

Considering the real vehicle model, there are several forces and contributes exchanged from the chassis on the wheels.
For the evaluation of the vehicle dynamics, a subdivision of the whole vehicle system into groups is commonly used. In particular, it could be convenient to study the individual dynamics of the subsystems described in the following paragraphs.

2.1.1 Wheel Loads

Wheels experience several kinds of loads, which greatly influence the forces exerted between the tires and the road at the ground contact point.
Mainly, there are the contributes of the vertical loads acting on each wheel, which can be summed up as static load, lateral load and longitudinal load, and the aerodynamics forces.

First of all, the static vertical forces are distributed on the wheels in resting state and they are attributed to the vehicle mass. The repartition of the weights mainly concerns front and rear axles according to the following equations:

$$F_{z0,F} = \frac{mgl_r}{L} \tag{2.1}$$

$$F_{z0,R} = \frac{mgl_f}{L} \tag{2.2}$$

Where the l_f and l_r represent the distance of the vehicle Centre of Gravity (CoG) respectively from the front axle and the rear one, $L = (l_f + l_r)$ is the total length given by the front and rear track length, m is the mass of the vehicle body concentred in the CoG of the vehicle and g is the gravitational acceleration.

Secondary, the lateral load transfer is manifested with a transfer of the weight from the inner to the external wheels. Neglecting the effects of suspensions and vehicle roll motion, the unique contribute is only due to the lateral acceleration on the vehicle CoG. Hence, the lateral load transfer can be simply represented by the formula below:

$$F^{y}_{z,F/R} = \frac{mha_y}{t_{wF/R}} \tag{2.3}$$

Where h is the vertical distance from the vehicle CoG to the ground.

Then, the wheels experience also the longitudinal load transfer which occurs due to the acceleration on the vehicle CoG along the X-axis in case of vehicle acceleration and braking. Neglecting again the suspension effects, the equations demonstrate a linear proportionality with the longitudinal acceleration a_x:

$$F_{z,F}^{x} = -\frac{mh|a_x|}{L} \tag{2.4}$$

$$F_{z,R}^{x} = +\frac{mh|a_x|}{L} \tag{2.5}$$

Finally, the last contribute is given by the aerodynamic force, which is acting on the centre of mass of the vehicle and which is composed of a longitudinal component and a vertical one:

$$F_x areo = \frac{1}{2}\rho C_l A v_x^2 \tag{2.6}$$

$$F_z areo = \frac{1}{2}\rho C_l A v_x^2 \tag{2.7}$$

Where ρ is the air density, v_x is the longitudinal velocity of the vehicle, C_l is the coefficient of lift (also named drag coefficient) and A is the surface of the chassis. Generally, for the estimation of the aerodynamic proprieties of a vehicle, CFD simulation tools are usually employed due to their evaluation complexity.

Summing up, the final equations which describe the vertical loads on the wheels, and then of course on the tires, are:

$$F_{Z,FL} = \frac{1}{2}F_{z0,F} - \frac{1}{2}F_{z,F}^{x} + \frac{1}{2}F_z^y + \frac{1}{4}F_z areo \tag{2.8}$$

$$F_{Z,FR} = \frac{1}{2}F_{z0,F} - \frac{1}{2}F_{z,F}^{x} - \frac{1}{2}F_z^y + \frac{1}{4}F_z areo \tag{2.9}$$

$$F_{Z,RL} = \frac{1}{2}F_{z0,R} - \frac{1}{2}F_{z,R}^{x} + \frac{1}{2}F_z^y + \frac{1}{4}F_z areo \tag{2.10}$$

$$F_{Z,RR} = \frac{1}{2}F_{z0,R} - \frac{1}{2}F_{z,R}^{x} - \frac{1}{2}F_z^y + \frac{1}{4}F_z areo \tag{2.11}$$

2.1.2 Wheel dynamics

Furthermore, it is possible to express the dynamics of the wheels studying the equilibrium equations of the wheel rotating, which describe the forces and moments acting on them.

It is sufficient to conduct the analysis on a single wheel, having the centre of mass of the wheel concentred in its centre and a single degree of freedom due to the rotation of the wheel. Other assumption to take in consideration are:

- The forces acting on the wheel are transmitted to its wheel centre.
- The torque causing traction and the torque due to braking are collected as a unique torque T_{wheel} thanks to the presence of torque vectoring and electrical motor, which actuate on the wheel the total desired torque.
- Neglection of rolling resistance.

Thus, the angular acceleration is defined as:

$$\dot{\omega} = \frac{T_{wheel} - R_{EM}F_x - M_y}{J_w} \tag{2.12}$$

Where T_{wheel} is the torque acting on the wheel after being multiplied by the transmission ration τ from the motor to the wheel, R_{EM} is the effective rolling radius of the wheel obtained as the average between the unloaded vehicle and the wheel radius subjected to deformations due to vertical forces, and M_y is the moment of the wheel around the Y-axis with reference frame in the centre of the wheel.

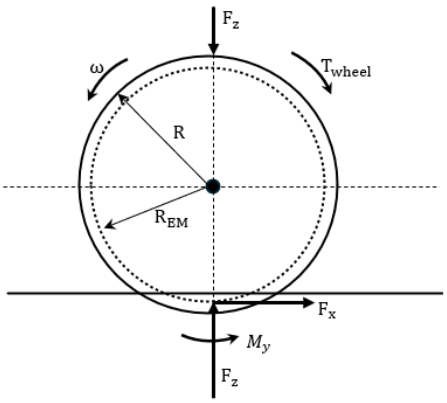

Figure 2.1 – Wheel dynamics

2.1.3 Tire modelling

Another important role in the vehicle dynamics is covered by the tire characteristics. However, tires behaviour definition is very complex due to their high non-linearities. There exist several tires models, but one of the most complete and used in literature is the Pacejka tire model. [14]
Specifically, it is a semi-empirical model which describes the longitudinal and lateral forces applied to the tires as a non-linear function of the longitudinal slip k and the side slip angle α.
The standard form of the Pacejka tire model is:

$$F_{i0} = D_i(C_i \arctan\,(B_i s_i - E_i(B_i s_i - arctan(B_i s_i)))) \tag{2.13}$$

Where the coefficients B, C, D, E are respectively the stiffness factor, shape factor, peak value and curvature factor and they are set according to the characteristics of the tires; while the s_i stays for the tire slip angles.
A more detailed definition of the longitudinal and lateral tire forces is expressed as:

$$F_{x0} = \mu_x F_x(C_x \arctan\,(B_x k - E_x(B_x k - arctan(B_x k)))) \tag{2.14}$$

$$F_{y0} = \mu_y F_y(C_y \arctan\,(B_y \alpha - E_y(B_y \alpha - arctan(B_y \alpha)))) \tag{2.15}$$

Where μ_x and μ_y are the longitudinal and lateral friction coefficient of the tires.
Due to the highly non-linearity characteristics of the Pacejka model, it is then fundamental to keep the working point of the tires in the linear region, limiting the values of the tire slipping to small values. Specifically, the longitudinal and lateral slip angles are obtained from:

$$k = \frac{R_{EM}\omega - V_{x,wheel}}{V_{x,wheel}} \tag{2.16}$$

$$\alpha = \arctan\left(\frac{V_{y,wheel}}{V_{x,wheel}}\right) \tag{2.17}$$

2.2 Single-Track bicycle vehicle model

For the development of the MPC and TVC in this thesis work, the study of the lateral dynamics of the vehicle is fundamental. However, to limit the complexity of the computations, it is necessary to reach a compromise between a complete vehicle analysis and a suitable simplification of the model, applicable for this project.

Firstly, the motion of the car is supposed to be planar along the XY plane, and any motion along the Z-axis can be neglected. This means that total chassis motion can be sufficiently described by three degrees of freedom (3 DOF), considering the movement of the centre of gravity of the vehicle and the orientation of the car, defined by the Yaw Angle. More commonly, the orientation of the vehicle is expressed as the rate of change of the Yaw Angle ψ in time, also known as Yaw Rate r. [15]
From these simplifications, the vehicle lateral dynamics can be easily represented with a 3-DOF non-linear single-track bicycle model with a linearized model of tires. In particular, the choice of this model type is strategic since it constitutes properly the trade-off between accuracy and simplicity of the model with respect to the reality. [16]

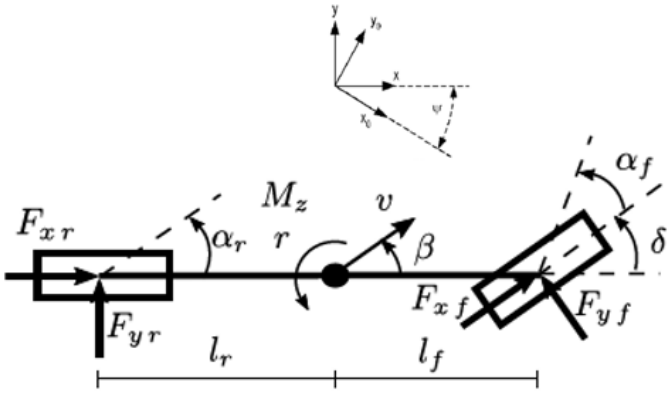

Figure 2.2 – Vehicle bicycle model [16]

The bicycle model is very popular in literature, and it can be easily obtained considering the following assumptions:

- Vehicle body considered as a rigid body with vehicle mass centred in its CoG.
- Wheels are lumped together on the axles.

- Vehicle drives on a flat surface.
- Load transfer can be neglected.
- Wheels forces act transmitted to the vehicle body CoG.
- Roll and pitch motions are neglected.
- Aerodynamics effects are neglected.
- Tire forces are simplified to be linear.
- Small tire slip angles.
- Steering due to only front wheels.
- Constant vehicle longitudinal velocity.
- Combined slip can be neglected.
- Self-aligning moment can be neglected.

Accepting these simplifications, the single-track model could be represented with a combination of non-linear kinematic equations and dynamic ones. (2.18) – (2.23)

For what regards the kinematic model, it aims to describe the position of the vehicle CoG on the XY plane. Differently, the dynamics of the vehicle model is sufficiently described exploiting the 3 DOF of the model and it is useful to represent the chassis motion in the plane, neglecting the motion along the vertical axis. Additionally, the vehicle dynamics comprehends the external moment M_z, which is attributed to the action of the Torque Vectoring Controller in the low level.

As result, equations describing the kinematics and dynamics of the bicycle model can be written as below:

$$\dot{X} = V_x \cos(\psi) - V_y \sin(\psi) \tag{2.18}$$

$$\dot{Y} = V_x \sin(\psi) + V_y \cos(\psi) \tag{2.19}$$

$$\dot{\psi} = r \tag{2.20}$$

$$\dot{V_x} = \frac{1}{m}\left(F_{xf}cos\delta - F_{yf}sin\delta + F_{xr}\right) + rV_y \tag{2.21}$$

$$\dot{V_y} = \frac{1}{m}\left(F_{xf}sin\delta + F_{yf}cos\delta + F_{yr}\right) - rV_x \tag{2.22}$$

$$\dot{r} = \frac{1}{I_z}(F_{xf}l_f sin\delta + l_f F_{yf} cos\delta - l_r F_{yr} + M_{zTVC}) \tag{2.23}$$

where V_x and V_y are the longitudinal and lateral velocities, expressed as components of the velocities in the mobile reference frame, and the ψ is the angle between the mobile reference frame centred in the vehicle CoG and the original refence frames.
Instead, m is the mass of vehicle, I_z is the yaw inertia and δ is the steering angle of the front wheels, F_x and F_y are the forces at the tyres due to interaction with the ground.

In order to transform the equations described below in a linear form, it can be actuated a linearization of the lateral tire forces, derived from the Pacejka tires model. The hypothesis to be accepted for this scope are listed below:

- F_y lateral tire forces are null for straight line driving.
- Small side slip angles, to guarantee the exploit of the tire model curve in its linear region.
- Cornering stiffness is considered constant, to neglect the dependency from the vertical load, assuming their average value on each wheel, and the road adhesion coefficient.

Hence, the lateral forces on the wheels, based on the linearization of the Pacejka model, can be expressed as a function of the vertical load and the sideslip angle of the tire $\alpha_{F/R}$. The, the lateral forces can be geometrically computed as a function of the longitudinal velocity V_x, yaw rate r, steering angle δ and vehicle sideslip angle β:

$$F_{yf} = 2C_f\alpha_F = 2C_f\left(\delta - \frac{V_y + l_f r}{V_x}\right) \tag{2.24}$$

$$F_{yr} = 2C_f\alpha_R = 2C_f\left(-\frac{V_y - l_r r}{V_x}\right) \tag{2.25}$$

having the linearized the sideslip angles of the tire:

$$\alpha_F = \delta_F - \frac{l_F\psi}{v_x} - \beta \tag{2.26}$$

$$\alpha_R = \frac{l_R\psi}{v_x} - \beta \tag{2.27}$$

To be noticed that in this single-track vehicle model, we have supposed that the vehicle steering is due to only the front steering wheel δ_F, having in this case the

vehicle side-slip angle β being small. In addition, it can be noticed also that the Ackermann turning geometry of a double track model can be neglected, since the front steering wheels are lumped together. Thus, the front wheel steering angle is obtained as: [15]

$$\delta \approx \delta_F \approx \delta_o = \frac{L}{R} \tag{2.28}$$

Which doesn't require any increase or decrease correction, since we are supposing the vehicle has a neutral steering behaviour, with an understeer gradient K_u close to zero.

Finally, considering all the hypothesis done up to now, and supposing also small steering wheel angle δ, to remove the non-linear contributes due to the cosine and sine, the equation (2.18) – (2.23) can be simplified in the form:

$$\dot{X} = V_x \cos(\psi) - V_y \sin(\psi) \tag{2.29}$$

$$\dot{Y} = V_x \, sin(\psi) + V_y \, cos(\psi) \tag{2.30}$$

$$\dot{\psi} = r \tag{2.31}$$

$$\dot{V_x} = \frac{1}{m}\left(F_{xf} + F_{xr}\right) + rV_y \tag{2.32}$$

$$\dot{V_y} = \frac{1}{m}\left(F_{yf} + F_{yr}\right) - rV_x \tag{2.33}$$

$$\dot{r} = \frac{1}{I_z}(l_f F_{yf} - l_r F_{yr} + M_{zTVC}) \tag{2.34}$$

2.3 State space model for the MPC and TVC problems

The objective of this analysis is to derive from the previous equations the linear system to be used in the MPC and TVC controllers. For the design of the control system, one of the most important steps is to opportunely derive the space-state representation of the system, whose linear continuous time form is represented by:

$$\dot{x} = Ax + Bu \tag{2.35}$$

$$y = Cx + Du \tag{2.36}$$

The state-space model is very useful for the correct definition of the control actions since it allows to clearly understand the input and output variables of the controller and the state variables which are involved and change with time. The y is the output vector, u is the vector collecting all the inputs, while x is the vector comprehending all the state variables, expressed also in derivative form to better evaluate evolution of the states in time.

2.3.1 MPC state space equations

The state-space model used in the linear MPC controller is composed of the state vector x, comprehending the following variables:

$$x = \left[X, Y, \psi, V_x, V_y, r\right]^T \tag{2.37}$$

Since, the vehicle is assumed to move at constant longitudinal velocity, the derivative of the longitudinal velocity is assumed to be null. The remaining variables are defined in the formulas (2.29) - (2.34), with the only difference that in the yaw rate state $\dot{r}$ the contribute of the additional moment generated by the TVC is not considered. This is because its action aims to correcting the evolution of the MPC in order to push the plant working according to the predictive internal model in the MPC, correcting all the errors due to linearization and imprecision.
In conclusion, the state space formulation in linear continuous time form for the MCP problem defined as below, where A is the state matrix and B is the input matrix:

$$\begin{bmatrix} \dot{X} \\ \dot{Y} \\ \dot{\psi} \\ \dot{V}_x \\ \dot{V}_y \\ \dot{r} \end{bmatrix} = \begin{bmatrix} 0 & 0 & 0 & 1 & 0 & 0 \\ 0 & 0 & V_{x0} & 0 & 1 & 0 \\ 0 & 0 & 0 & 0 & 0 & 1 \\ 0 & 0 & 0 & 0 & 0 & 0 \\ 0 & 0 & 0 & 0 & -\frac{2(C_f + C_r)}{mV_{x0}} & -\frac{2(C_f l_f - C_r l_r)}{mV_{x0}} - V_{x0} \\ 0 & 0 & 0 & 0 & -\frac{2(C_f l_f - C_r l_r)}{I_z V_{x0}} & -\frac{2(C_f l_f^2 + C_r l_r^2)}{I_z V_{x0}} \end{bmatrix} \begin{bmatrix} X \\ Y \\ \psi \\ V_x \\ V_y \\ r \end{bmatrix} + \begin{bmatrix} 0 \\ 0 \\ 0 \\ 0 \\ \frac{2C_f}{m} \\ \frac{2C_f l_f}{I_z} \end{bmatrix} [\delta] \tag{2.38}$$

2.3.2 TVC space state equations

For the TVC problem, the two states exploited for study the car's lateral dynamics are the vehicle side-slip angle and the yaw rate, as defined in the equations: [16]

$$\dot{\beta} = \frac{1}{mV_x}\left(F_{y,F} + F_{y,R}\right) - r \tag{2.39}$$

$$\dot{r} = \frac{1}{I_z}\left(l_f F_{y,F} - l_r F_{y,R}\right) + M_z \tag{2.40}$$

Thus, recurring to the linearized Pacejka tire's model and assumption explained in this chapter, the state space system for the TVC problem formulation is: [16]

$$\begin{bmatrix} \dot{\beta} \\ \dot{r} \end{bmatrix} = \begin{bmatrix} -\frac{2(C_f + C_r)}{mV_x} & -1 + \frac{2(C_r l_r - C_f l_f)}{mV_x^2} \\ \frac{2(C_r l_r - C_f l_f)}{I_z} & -\frac{2(C_f l_f^2 + C_r l_r^2)}{I_z V_x} \end{bmatrix} \begin{bmatrix} \beta \\ r \end{bmatrix} + \begin{bmatrix} \frac{2C_f}{mV_x} \\ \frac{2C_f l_f}{I_z} \end{bmatrix} \delta + \begin{bmatrix} 0 \\ \frac{1}{I_z} \end{bmatrix} M_z \tag{2.41}$$

Where β is the sideslip angle, which is the angle between the orientation of the chassis and the vector of instantaneous longitudinal velocity centred in the CoG of the vehicle.
As it is reported into the continuous-time state-space model, the contributes which give the derivative of the state vector are coherent with the standard representation usually employed in torque vectoring controller [2], [16]:

$$\dot{x} = [A]x + [B]M_z + [Bd]\,\delta \tag{2.42}$$

Where it is possible to denote:
- state vector with the controlled states $x = [\beta\ r]^T$, and the respective input matrix A.
- the input M_z, which is the corrective action given by the TVC controller, and the respective input matrix B.
- the steering angle δ as a disturbance and the relative disturbance matrix Bd.

3 MPC and TVC control strategy

As already mentioned in the introductive chapter, the general architecture foreseen for an autonomous vehicle collects more than one layer which can be summed up into:

- a perception layer, for the detection of the surrounding environment, including the track lanes and eventual obstacles.
- a reference planning layer, for the generation of the trajectory to be followed for by the vehicle.
- a control layer, which represents the low-layer and includes the control strategies and employed for from the actuation of the steering command, braking and traction forces aimed to control the vehicle dynamics and to guarantee the desired behaviour. [18]

The main controllers described in this chapters are developed to be integrated in the control layer of the prototype's architecture, and its general scheme is represented in Figure 3.1.
Firstly, the control system is composed of a simple PI controller for maintain the longitudinal vehicle velocity at the reference speed, thus generating the total braking and traction total force required to be allocated to the wheels. The presence of a linear Model Predictive Control (MPC) block, controlling the lateral vehicle dynamics, satisfies the autonomous capability of path tracking and supersedes the steering action by the driver. Hence, in this case of study the longitudinal and lateral dynamics are separated in order to avoid their reciprocal influence and to not exceed in the complexity of the MPC computations.
Moreover, a Torque Vectoring block, whose development is the main scope of this thesis work, contributes to the whole functioning of the control system. In fact, its basilar action is the vectorization of the wheel motor torque to satisfy the traction/braking force required by the longitudinal controller and, moreover, contributes to the MPC in controlling the lateral dynamics of the vehicle by generating ad an additional yaw moment. Finally, a block simulating a mechanical

braking intervenes in the case the regenerative braking by the torque vectoring is not sufficient.

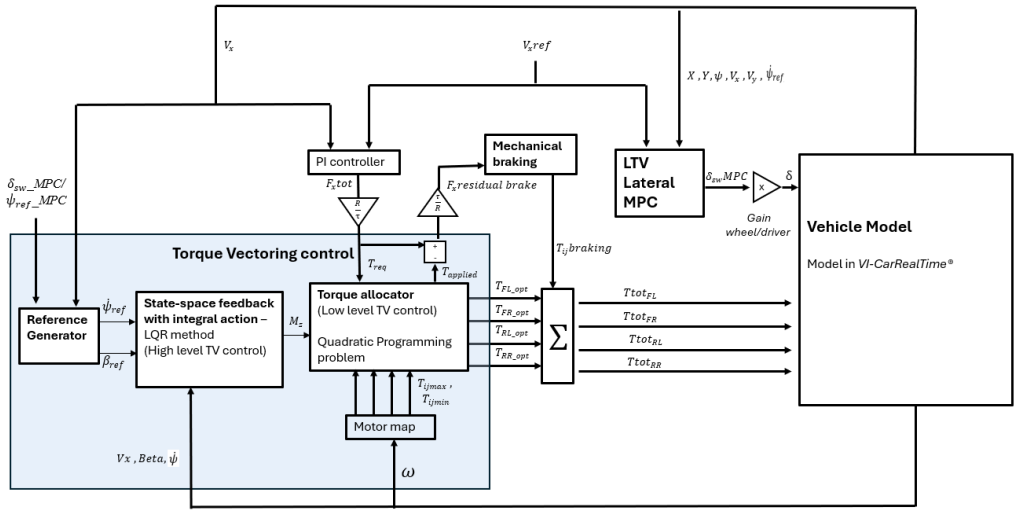

Figure 3.1 – Control layer architecture

3.1 Model Predictive Control

As already mentioned, the aim of the MPC in this thesis is to control the lateral dynamics of the vehicle and find the optimal sequence of discrete steering angle at wheels to achieve the path tracking goal, following the reference trajectory planned from the detection of the unknown environment surrounding the prototype. To be noticed that the following MPC design approach, employed in this thesis, has been described also in [19], which describes in details the optimal control problem and its real-time implementation on the prototype in common with the two thesis works.

3.1.1 Reference trajectory tracking

The actuation of the MPC strategy is focused on the tracking of the reference path in the most accurately and less computational way. A good strategy for an optimal MPC implementation is converting the coordinates of the planned trajectory from the global reference frame RF^0, situated into the point of the vehicle start position and remaining fixed, to the local mobile reference frame RF^1 which moves attached to the vehicle CoG.

Both the two reference frames are compliant with the ISO 8855-2011 standard. The difference is that in the mobile reference frame RF^1 the origin is collocated in the centre of gravity (CoG) of the vehicle, the longitudinal x-axis is directed along the centre line of the vehicle, the vertical z-axis is perpendicular to the ground when the vehicle is steady and pointing upward and the y-axis represents the righ-handled orthogonal reference system with the other two axis just described.

The application of the transformation matrix allows to change a point definition from the fixed reference frame to the mobile one. Specifically, the transformation matrix is a combination of the Rotation matrix and Translation matrix at the instant i. The rotation matrix describes the result of a rotation around the z-axis of a datum angle θ_i, instead the translation vector described a rigid translation given by the distance vector between the two frames' origins.

$$R_{1,k}^{0} = \begin{bmatrix} cos\theta_i & -sin\theta_i & 0 \\ sin\theta_i & cos\theta_i & 0 \\ 0 & 0 & 1 \end{bmatrix} \tag{3.1}$$

$$t_{01}^{0} = [X_i \quad Y_i \quad 0]^T \tag{3.2}$$

The result of the combination is expressed by the Transformation Matrix reported in the formula below, and it describes how to compute the transformation of the coordinates of a point in the frame RF^0into the mobile frame RF^1:

$$T_{1,k}^{0} = \begin{bmatrix} cos\theta_i & -sin\theta_i & 0 & X_i \\ sin\theta_i & cos\theta_i & 0 & Y_i \\ 0 & 0 & 1 & 0 \\ 0 & 0 & 0 & 1 \end{bmatrix} \tag{3.3}$$

The main advantage of implement such transformation is that choosing the mobile local frame, centred in the CoG of the vehicle, it is possible to get rid of the initial states of the state space matrix, having the X and Y position and the yaw angle equal to zero.

Hence, expressing the points of the reference trajectory in the same reference local frame of the vehicle, makes the MPC more robust to disturbances, improving t accuracy and reliability.

At each iteration, the MPC tries to adjust the steering angle for achieving the optimal steering sequence which minimize the cross-track error, defined as the distance between the vehicle position CoG and the reference trajectory. In order to determine the cross-track error, the strategy employed recurs to the evaluation

of the linear interpolation of the two closest points and the perpendicular line passing from the CoG of the vehicle.
With this implementation, it is possible to predict the distance covered by the vehicle and to predict its state position as defined in the MPC state space system. In fact, considering the vehicle moving at constant longitudinal velocity, the distance between the current and the estimated next position of the car is determined by the multiplication of the longitudinal speed V_x and the time constant of the MPC $T_s = 0.05s$. So, the predicted state position of the vehicle is obtained from the intersection of the interpolation line of the two point of the trajectories and a circumference centred in the CoG of the car and having a radius equal to the distance predicted as explained. Finally, the discretization of the reference trajectory, required by the MPC, is obtained by the application of the methodology explained in a recursive way.

3.1.2 MPC Optimization Control Problem (OCP) formulation

The linear time invariant (LTI) MPC described hereinafter considers the state space system which can is expressed by the linear continuous time model of the vehicle, as already described in the previous chapter:

$$\begin{bmatrix} \dot{X} \\ \dot{Y} \\ \dot{\psi} \\ \dot{V}_x \\ \dot{V}_y \\ \dot{r} \end{bmatrix} = \begin{bmatrix} 0 & 0 & 0 & 1 & 0 & 0 \\ 0 & 0 & V_{x0} & 0 & 1 & 0 \\ 0 & 0 & 0 & 0 & 0 & 1 \\ 0 & 0 & 0 & 0 & 0 & 0 \\ 0 & 0 & 0 & 0 & -\frac{2(C_f + C_r)}{mV_{x0}} & -\frac{2(C_f l_f - C_r l_r)}{mV_{x0}} - V_{x0} \\ 0 & 0 & 0 & 0 & -\frac{2(C_f l_f - C_r l_r)}{I_z V_{x0}} & -\frac{2(C_f l_f^2 + C_r l_r^2)}{I_z V_{x0}} \end{bmatrix} \begin{bmatrix} X \\ Y \\ \psi \\ V_x \\ V_y \\ r \end{bmatrix} + \begin{bmatrix} 0 \\ 0 \\ 0 \\ 0 \\ \frac{2C_f}{m} \\ \frac{2C_f l_f}{I_z} \end{bmatrix} [\delta] \quad (3.4)$$

Due to the nature of the proposed control system and its implementation on the prototype, it is necessary to derive discrete time formulation applying the zero-order or Euler discretization to the state-space system in the continuous form [18] defined in (3.4). Then, the discrete time form of matrices is defined as:

$$\begin{aligned} A_d &= (I - T_s A_c)^{-1} \\ B_d &= T_s A_d B_c \end{aligned} \quad (3.5)$$

Where T_s is the sampling time used for the discretization.
The standard form of a discrete time state-space system is:

$$\begin{aligned} x[k+1] &= A_d x[k] + B_d u[k] \\ y[k] &= C_d x[k] + D_d u[k] \end{aligned} \tag{3.6}$$

As presented in some literatures studies [17], it can be suitable for this case of study to consider the augmented state-space system which provides the prediction of the input $u[k+1]$, as expressed in the system below:

$$\begin{bmatrix} x[k+1] \\ u[k+1] \end{bmatrix} = \begin{bmatrix} A_d & B_d \\ 0 & I \end{bmatrix} \begin{bmatrix} x[k] \\ u[k] \end{bmatrix} + \begin{bmatrix} B_d \\ I \end{bmatrix} \Delta u[k] \tag{3.7}$$

Where the new input of the state-space system is actually the discrete variation of the steering angle Δu, and the augmented state-space vector is $[x, u]^T$. In fact, the predicted steering input at the next time instant can be represented as:

$$u[k+1] = u[k] + \Delta u[k] \tag{3.8}$$

From the forward-shifting of the input $u[k]$ of a time instant
As it is known, the MPC implementation allows to impose equality and inequality constraints to the state-variables and the inputs, according to the physical system to be modelled and the actual problem to be solved.[18] In this case, the hard inequality constraints for the vehicle position states x, y and ψ have been set to infinite for the low and up boundaries to allow the motion of the vehicle without any limitation in the planar space. Moreover, also the upper and lower constraints imposed for the longitudinal and lateral velocities and the yaw rate have been neglected, by setting their values to the infinite, since the controlling of the vehicle longitudinal and lateral speed is out of the scope of this MPC application.
More strictly constraints have been foreseen for the input steering angle u, whose values are accepted only in a range $[-20°; +20°]$. Additionally, a second constraint has been applied to the steering input Δu in order to consider the low-pass filter behaviour of the real steering actuator mounted on the prototype. More precisely, a limitation of the speed of actuation at frequencies higher than the cut-off frequency at 4Hz has been imposed. The same constraints are established in [19] too.

In the framework of the proposed MPC, the Optimal Control Problem (OCP), expressed in discrete form, is formulated as below:

$$\min_{\Delta u} J = \sum_{k=0}^{N} \left(\|x_k - x_{ref,k}\|_Q^2 + \|u\|_{R_u}^2 + \|\Delta u\|_{R_{\Delta u}}^2 \right) \tag{3.9}$$

Subjected to

$x_{k+1} = A_d x_k + B_d u_{k+1} \quad k = 0, \dots, N$

$u_{k+1} = u_k + \Delta u_k \quad k = 0, \dots, N$

$y_k = C_d x_k$

$\Delta u_0 = 0$

$x_0 = \hat{x}$

$u_0 = \hat{u}$

$x_{min} \leq x_k \leq x_{max} \quad k = 1, \dots, N$

$u_{min} \leq u_k \leq u_{max} \quad k = 1, \dots, N$

$\Delta u_{min} \leq \Delta u_k \leq \Delta u_{max} \quad k = 1, \dots, N$

Where J is the cost function that the OCP aims to minimize, the equality constraints are defined according to the kinematics and dynamics of the bicycle model, and the hard inequality constrains according to the expected performances already described. The presence of the sum operator indicates that the optimal solution is comprehensive of all the steps, indicated by k, from zero to the total number of steps N of the prediction horizon. [18] To be notice, that in this formulation the prediction horizon and the control horizon have the same value of Finite Time Horizon. The Q, R_u and $R_{\Delta u}$ are the weighting matrices for the tuning of the states and input variables to regulate the path tracking performances by the vehicle. Finally, the initial conditions of the states and the input variables are set to the estimated or measured values ($\hat{x}$ and $\hat{u}$) from the plant or the sensors on the vehicle.

3.1.3 MPC problem application and solving

For the application of the MPC to the desired path tracking goal, the states variables to be controlled are only the vehicle position along the plane defined by the X and Y-axis. Hence, the discrete state-space system, considering also the steering angle δ as the input, can be explicated as:

$$\begin{bmatrix} x[k+1] \\ \delta[k+1] \end{bmatrix} = \begin{bmatrix} A_d & B_d \\ 0 & I \end{bmatrix} \begin{bmatrix} x[k] \\ \delta[k] \end{bmatrix} + \begin{bmatrix} B_d \\ I \end{bmatrix} \Delta\delta[k] \tag{3.10}$$

$$y[k] = C_d x[k] = [1 \quad 1 \quad 0 \quad 0 \quad 0 \quad 0]x[k] \tag{3.11}$$

Moreover, the discrete points of the reference trajectory are transformed from the global reference frame RF^0 to the local one RF^1, increasing the MPC computations accuracy, by the application in the on the transformation matrix defined as:

$$T_0^1 = \begin{bmatrix} cos\psi_0 & sin\psi_0 & 0 & -X_0 cos\psi_0 - Y_0 sin\psi_0 \\ -sin\psi_0 & cos\psi_0 & 0 & X_0 sin\psi_0 - Y_0 cos\psi_0 \\ 0 & 0 & 1 & 0 \\ 0 & 0 & 0 & 1 \end{bmatrix} \tag{3.12}$$

Concluding, the optimization control problem defined in (3.9) can be reformulated as:

$$\min_{\Delta u} J = \sum_{k=0}^{N} \left((y_k - y_{ref,k}) Q (y_k - y_{ref,k}) + R_u \delta_k^2 + R_{\Delta u} \Delta\delta_k^2 \right) \tag{3.13}$$

Subjected to

$x_{k+1} = A_d x_k + B_d \delta_{k+1} \quad k = 0, \dots, N$

$\delta_{k+1} = \delta_k + \Delta\delta_k \quad k = 0, \dots, N$

$y_k = C_d x_k$

$\Delta\delta_0 = 0$

$x_0 = \hat{x}$

$\delta_0 = \hat{\delta}$

$\delta_{min} = -20° \leq \delta_k \leq \delta_{max} = 20° \quad k = 1, \dots, N$

$\Delta\delta_{min} = -2\pi(4Hz)T_s \leq \Delta\delta_k \leq \Delta\delta_{max} = 2\pi(4Hz)T_s \quad k = 1, \dots, N$

For solving the optimization control problem in MATLAB/Simulink, it is necessary to explicit the OCP in a Quadratic Programming problem formulation, aiming to find the optimal solution by minimizing the objective function with the form of:

$$\min J = \left(\frac{1}{2} z^T H z + f^T z \right) \tag{3.14}$$

Subjected to

$$LB \leq Az \leq UB$$
$$A_{eq}z \leq b_{eq}$$
$$Az \leq b$$

Where the optimization variable z is populated by all the states of the state vector x and all the input included into the prediction horizon $Hp = N$ of the optimization problem, and it is defined as [19]:

$$z = [x_0 \quad x_1 \cdots \quad x_N \quad \delta_0 \quad \delta_1 \cdots \quad \delta_N \quad \Delta\delta_1 \cdots \quad \Delta\delta_N \,] \tag{3.15}$$

The standard formulation in quadratic programming problems foresees an arrangement of the cost function which distinguishes the linear terms, contained into the positive semidefinite vector f, and the quadratic terms, collected into the positive semidefinite quadratic objective matrix H. Specifically, the H matrix contains on its diagonal the weight matrices of the states and the inputs contained in the variable z. While the vector f contains the reference states multiplied by the relative elements of the weight matrix Q.

$$H = \begin{bmatrix} Q_0 & & & & & & & & \\ & \ddots & & & & & & & \\ & & Q_N & & & & & & \\ & & & R_{u0} & & & & & \\ & & & & \ddots & & & & \\ & & & & & R_{uN} & & & \\ & & & & & & R_{\Delta u1} & & \\ & & & & & & & \ddots & \\ & & & & & & & & R_{\Delta uN} \end{bmatrix} \tag{3.16}$$

$$f = \begin{bmatrix} -Q_0 x_{0,ref} \\ \vdots \\ -Q_N x_{N,ref} \\ [0]_{nu} \\ [0]_{ndu} \end{bmatrix} \tag{3.17}$$

Where nu and ndu stays for the number of the inputs δ and $\Delta\delta$, hence they are both equal to the unitary.
Instead, the constraint matrix A contains both the linear equalities and inequalities constraints related to the states and the inputs along the prediction horizon,

considering the discrete state-space representing the vehicle dynamics and evolving in time, a detailed description is in [19]. The LB and UB are respectively the lower bounding vector and the upper bounding vector, which provide the bounds for the product of the constraint matrix A with the optimization variable z, according to already done considerations on the states and the inputs constraints. The bounding vectors can be explicated as below [19], where nx stays for the number of the states in the optimization vector x.

$$LB = [x_0 \quad u_0 \quad [0]_{nx} \quad [0]_{nu} \quad [0]_{ndu} \quad x_{min} \quad u_{min} \quad \Delta u_{min}]^T$$
$$UB = [x_0 \quad u_0 \quad [0]_{nx} \quad [0]_{nu} \quad [0]_{ndu} \quad x_{max} \quad u_{max} \quad \Delta u_{max}]^T$$

3.2 Torque Vectoring

The main scope of this activity is the development of a Torque Vectoring Controller which consists in controlling the in-wheel motor torque.
As it is already mentioned in the previous paragraphs, the main objective of the Torque Vectoring is the distribution of the driving and braking forces between the wheels in order to generate an additional corrective yaw moment M_z. In fact, instead of an equal distribution of the torque on the wheels, an opportune split of the required torque on the wheels would contribute to improve the performances of the vehicle, especially in critical cornering situations.
The overall control architecture of Torque Vectoring proposed in this thesis is mainly composed by three subsystems, as many studies in literature present [2], [3], [16]:

- Reference Generator, with the aim of generating the desired yaw rate reference and side-slip angle reference.
- High-Level TV Controller, which generates in output the opportune corrective yaw moment M_z.
- Torque Allocator, which constitutes the low-level controller of the TV and distributes optimally the additional yaw moment generated to the high-level controller increasing and/or decreasing the torque at each wheel.

A complete scheme of the just described Torque Vectoring architecture is reported in the Figure 3.2 and it with better explained as follows.

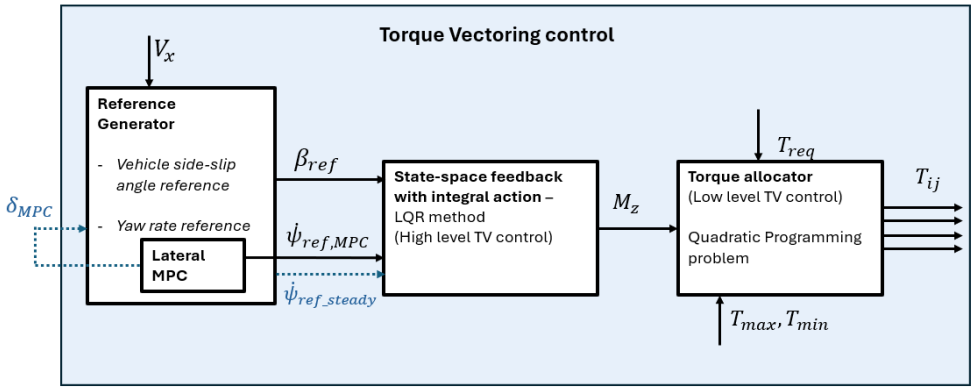

Figure 3.2 – Torque Vectoring control architecture

3.2.1 Reference generator

In this first block, the reference yaw rate and the reference vehicle side-slip angle are computed from the vehicle dynamics.

Generally, in literature the vehicle is analysed in a situation of steady state cornering, hence reducing the complexity of the computation.
In steady state cornering, the yaw rate can be easily calculated dividing the longitudinal velocity of the vehicle V_x by the radius of the path R:

$$r_{reference} = \frac{V_x}{R} \tag{3.18}$$

Moreover, the inverse of the geometric radius of the path R can be proportional to the following parameters:

$$\frac{1}{R} = \frac{\delta}{L + K_u V_x^2} \tag{3.19}$$

Where the δ is the steering angle at the wheels, the L is the distance from the front to the rear wheels, and the K_u is the vehicle understeer gradient.
These last parameters determine the vehicle propension to an understeering or an oversteering behaviour, which is relevant when the vehicle faces cornering

situations. The understeering behaviour could be simply explained by the needing of the vehicle of increasing the steering wheel angle to follow a non-straight path; instead, in case of oversteering the steering wheel angle can be reduced.
The understeer gradient can be written as the difference between the ratio of the mass front axle on the front wheels cornering stiffness and the ratio of the mass rear axle on the rear wheels cornering stiffness:

$$K_u = \frac{m_f}{C_f} - \frac{m_r}{C_r} \tag{3.20}$$

Thus, when the K_u factor is positive vehicle has an understeering behaviour, when the K_u is negative vehicle is oversteering.
In this case of study, the understeer factor is assumed to be close to zero, supposing the vehicle having a neutral steering behaviour.
Finally, from the combination of the upper equations, the yaw rate reference in steady state cornering can be obtained as [16]:

$$r_{reference} = \frac{\delta \cdot V_x}{L + K_u V_x^2} \tag{3.21}$$

Where the steering angle δ is the optimal command generated by solving the optimal control problem of the MPC.
However, in this thesis the presence of the lateral MPC controller has been furtherly exploited to provide the vehicle yaw rate reference instead of the steady-state reference given by the formula (3.21). In fact, for the computation of the optimal steering angle δ, which is the output of the MPC according to the given reference path, the MCP computes the evolution in time of its internal state-space (3.4) describing the vehicle dynamics. As already explained, the optimization variable z comprehends all the states and inputs along the prediction horizon of the OCP, from which then the predicted yaw rate state can be extracted.
The employment of the predicted yaw rate reference from the MPC allows to achieve better overall performances, since the Torque Vectoring acts correcting the actual yaw rate having a vehicle behaviour closer to the predicted one.
The other advantage is the consequent increase of the prediction's reliability from the MPC.
For this reason, the yaw rate reference generator block can be superseded taking the yaw rate reference directly from the MPC block, after having checked that consistency of the MPC predicted yaw rate respect to the values obtained from the steady state formula.

Anyway, the Reference Controller is needed for the computation of the vehicle's side-slip angle reference, which keeps the vehicle in the stability limits, by using [3], [20]:

$$\beta_{reference} = \beta_{max} tanh\left(\frac{\beta}{\beta_{max}}\right) \tag{3.22}$$

Using the following empirical formula for the slip-angle bound limit in which the tyre's forces still maintain a linear behaviour [15], [20]:

$$\beta_{max} = tan^{-1}(0.02\mu g) \tag{3.23}$$

Where μ is the road-tire coefficient of friction, assumed equal to 1 in our case, and g is the gravitational acceleration.

3.2.2 High Level TV Block: state-space feedback with Linear Quadratic Regulator (LQR) and integral action

Once the reference yaw rate and side-slip angle signals have been generated, a comparison with the actual values of this states is performed, getting the respective error quantities. Thus, the high-level TV controller has the scope of generating the additional torque moment M_z starting from the errors provided by the feedback signals.
Considering the single-track model of the vehicle the state model is derived as reported in equation (2.41) and, as already done for the MPC block in (3.6), the zero-hold discretization has been employed to obtain its discrete time state-space system:

$$\begin{gathered} x[k+1] = A_d x[k] + B_d M_z[k] + B d_d \delta[k] \\ y[k] = C_d x[k] + D_d u[k] = [0 \quad 1] x[k] + [0] M_z[k] \end{gathered} \tag{3.24}$$

Reminding that in this modelling of the vehicle's system the delta steering δ and the additional torque moment M_z are respectively considered as a disturbance and as the input of the state space model, the state vector x contains the side-slip angle β and the yaw rate r vehicle states, and the output y is due to only the yaw rate state contribute.

Many controllers in literature implement steady-state feedback with an integral action which aims to provide a zero steady-state error, thanks to the elimination of errors due to uncertainties in the internal model of the controller. [21]
Hence, the discrete time state-space system in (3.24) has been redefined in order to include the augmented state to consider the error between the actual yaw rate of the car, provided in feedback as an output of the plant, and the desired reference yaw rate coming from the MPC states evolution. The augmented discrete state-space system standard formulation is then:

$$\begin{aligned} x_{aug}[k+1] &= A_{aug,d}x_{aug}[k] + B_{aug,d}u[k] + Bd_{aug,d}d[k] \\ y_{aug}[k] &= C_{aug,d}x_{aug}[k] + D_{aug,d}u[k] \end{aligned} \tag{3.25}$$

From which the form applied in this sub-system is derived, explicating both the augmented state vector (3.26) and the state output (3.27):

$$\begin{bmatrix} x[k+1] \\ z[k+1] \end{bmatrix} = \begin{bmatrix} A_d & [0]_{2x1} \\ C_d & I_{1x1} \end{bmatrix} \begin{bmatrix} x[k] \\ y[k] - ref \end{bmatrix} + \begin{bmatrix} B_d \\ 0 \end{bmatrix} M_z[k] + \begin{bmatrix} Bd_d \\ 0 \end{bmatrix} \delta[k] \tag{3.26}$$

$$y[k] = [C_d \quad 0] \begin{bmatrix} x[k] \\ y[k] - ref \end{bmatrix} + [0 \quad 0]u[k] \tag{3.27}$$

Once derived the system for modelling the vehicle lateral dynamics to control with the TV, it is then possible to compute the input M_z by a minimization of the cost function:

$$J = \int_0^\infty (x^T Q x + uRu)\, dt \tag{3.28}$$

Subjected to
$lb \leq z \leq ub$
$A_{eq} z \leq b_{eq}$
$Az \leq b$

In the above formulation the weight matrices Q and R are computed starting from [20] and adapting the weight matrix Q for considering the integral contribution as:

$$Q = \begin{bmatrix} \frac{1}{\beta_{max}^2} & 0 & 0 \\ 0 & \frac{1}{\dot{\psi}_{max}^2} & 0 \\ 0 & 0 & \frac{1}{\dot{\psi}_{max}^2} \end{bmatrix} \tag{3.29}$$

$$R = \alpha \frac{1}{M_{z,max}^2} \tag{3.30}$$

Changing the values in these matrices it is possible to increase or decrease the relevance of the vehicle states or to penalize or not the effect of the input, hence properly tuning the two matrices the desired M_z input can be obtained. It can be noticed that the state weight matrix Q contains on its diagonal the maximum values of the side-slip and yaw rate vehicle states, as defined in (3.23) and (3.31), which maintains the car in stability condition: [15], [21]

$$\dot{\psi}_{max} = \frac{\mu g}{V_x} \tag{3.31}$$

Instead, the maximum value of yaw moment $M_{z,max}$ is obtained by exploited the maximum longitudinal force that the wheels can exert, considering the reduction ratio τ for passing from the motor torque to the torque applied at the wheels and the average effective rolling radius R_{EM}:

$$M_{z,max} = \frac{tw_f}{2} \left| F_{x,max}^{FR} - F_{x,max}^{FL} \right| + \frac{tw_r}{2} \left| F_{x,max}^{RR} - F_{x,max}^{RL} \right| \tag{3.32}$$

$$F_{x,max}^{ij} = \tau \frac{T_{ij,max}}{R_{EM}} \tag{3.33}$$

The solution which minimize the cost function in (3.28) can be obtained by implementing a Linear Quadratic Regulator (LQR) which solves the Riccati equation:

$$P = A'PA + Q - A'PB(R + B'PB)^{-1}B'PA \tag{3.34}$$

And finds the suitable values of $K = (R + B'PB)^{-1}B'PA$ which includes including both the proportional and the integral action:

$$K_{LQR} = [K_{o,\beta} \quad K_{o,r} \quad K_i] \tag{3.35}$$

Thus, it is possible to implement a state feedback whose control law includes both a proportional term referred to the vehicle side-slip and yaw rate states and an integral term for the elimination of the steady-state error, shown in the standard form in (3.36) and also explained in Figure 3.3:

$$u = -K_o x - K_i z \tag{3.36}$$

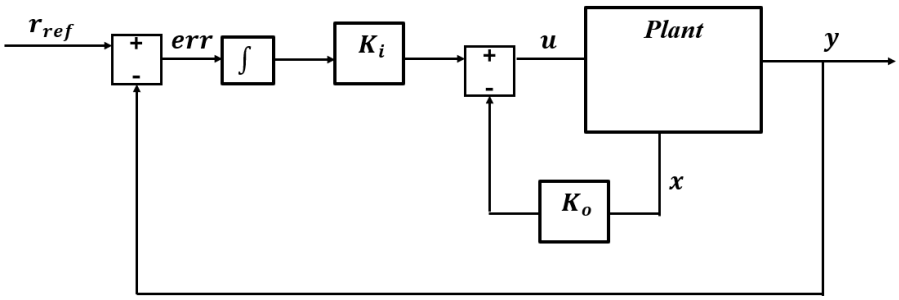

Figure 3.3 – State feedback with proportional and integral actions

In the end, the final employed control action is obtained by substituting the deviation of the states with respect their reference signals for the proportional contribution, as expressed in:

$$M_{z,LQR} = -K_o \begin{pmatrix} \beta - \beta_{ref} \\ r - r_{ref} \end{pmatrix} - K_i(r - r_{ref}) \tag{3.37}$$

In this way it is possible to furtherly increase the capability of the additional yaw moment M_z produced in eliminating the errors, allowing to have the vehicle states much closer to the reference signals.

3.2.3 Low Level TV Block: Torque Allocator with Quadratic Programming (QP) problem

In the framework of Torque Vectoring, the torque allocator block is generally used to effectively generate the desired additional vehicle moment, provided by the High-level block, by distributing the required torque opportunely to each in-wheel motors.

In this specific case, the TV Low-level subsystem solves a Quadratic Programming problem, whose implementation is inspired by the article in literature [20], to actuate an optimally torque allocation, guaranteeing the compliance with both the required torque T_{req} and the corrective yaw moment M_z from the upper layer. Concerning the T_{req}, it is generated by a PI controller which compares the reference longitudinal speed of the vehicle required by the driver and the current vehicle speed. Thus, the required torque can be both positive, in case of traction, and both negative, when the vehicle is decelerating within the limits of regenerative braking.

Entering in details of this block, the torque allocator implements a Quadratic Programming problem to obtain the unknown variables, trying to minimize a quadratic cost function subjected to linear equality and inequality constraints.
For what regards the variables, they are collected into the vector defined as below [20]:

$$x = \left[T_{FL}, T_{FR}, T_{RL}, T_{RR}, Sl_{Treq}, Sl_{Mz}\right]^T \tag{3.38}$$

which contains the motor torques at each wheel and two slack variables to avoid the infeasibility of the problem.
The scope of this method is to finds a vector solution to the quadratic cost function, standardly formulated as:

$$J = \min(\frac{1}{2}x^T Hx + f^T x) \tag{3.39}$$

Subjected to
$Ax \leq b$
$A_{eq}x = b_{eq}$
$LB \leq x \leq UB$

The aims of the implemented cost function are the minimization of:

a) the effects of the longitudinal load transfer weights (described in paragraph 2.1) to distribute a higher torque on the wheels which are subjected to more vertical load, since they can exert higher force due to their higher adhesion on the road.
b) The power losses due to the longitudinal tire slips.

In the quadratic cost function (3.39) the H is the positive semidefinite Hessian matrix which contains the quadratic terms and f is the positive semidefinite vector including the linear terms, as already described in section 3.1.3.
On one hand the variables in the vector are linearly multiplied by a the 6x1 positive semidefinite vector f, including the linear terms; on the other hand, the same vector x is quadratically multiplied by Hessian matrix, which has the form of a 6x6 diagonal positive definite matrix containing the quadratic terms. which In fact, according to the literature, the Hessian matrix can be exploited to study the convexity of the cost function, which is then convex, and it has the global minimum coincident with any local minimum if the sufficient condition of Hessian to be positive definite is satisfied. The H and f matrices are explicated as reported in literature. [20]

As it has already specified, the above cost function is subjected to equalities and inequalities, summed up as follows:

$$\begin{cases} A_{eq}x = b_{eq} \\ Ax \leq b \\ LB \leq x \leq UB \end{cases} \tag{3.40}$$

In this case of study, the equality constraints are then formulated considering the below equations:

$$\begin{cases} T_{FL} + T_{FR} + T_{RL} + T_{RR} + Sl_{Treq} = T_{req} \\ \tau\left[t_{WF}\left(\frac{T_{FR}}{R_{EM}} - \frac{T_{FL}}{R_{EM}}\right) + t_{wR}\left(\frac{T_{RR}}{R_{EM}} - \frac{T_{RL}}{R_{EM}}\right)\right] + Sl_{Mz} = M_z \end{cases} \tag{3.41}$$

From which the equality matrices are derived:

$$A_{eq} = \begin{bmatrix} 1 & 1 & 1 & 1 & 1 & 0 \\ -\tau\frac{t_{wF}}{R_{EM}} & \tau\frac{t_{wF}}{R_{EM}} & -\tau\frac{t_{wR}}{R_{EM}} & \tau\frac{t_{wR}}{R_{EM}} & 0 & 1 \end{bmatrix} \tag{3.42}$$

$$b_{eq} = \begin{bmatrix} T_{req} \\ M_z \end{bmatrix} \tag{3.43}$$

Additionally, the first inequality constraint in the equation (3.40) has the aim of guaranteeing the sign consistency of the request torque and yaw moment respectively with the actual torque and yaw moment applied. [20]

$$A_{eq} = \begin{bmatrix} -sign(M_{z,req})[-\tau\frac{t_{wF}}{R_{EM}} & \tau\frac{t_{wF}}{R_{EM}} & -\tau\frac{t_{wF}}{R_{EM}} & \tau\frac{t_{wF}}{R_{EM}} & 0 & 0] \\ -sign(T_{req})[1 & 1 & 1 & 1 & 0 & 0 \\ 0 & 0 & 0 & 0 & -sign(T_{req}) & 0 \\ 0 & 0 & 0 & 0 & 0 & -sign(M_{z,req}) \end{bmatrix} \quad (3.44)$$

$$b_{eq} = [0 \quad 0 \quad 0 \quad 0]^T \quad (3.45)$$

Differently, the second inequality in (3.40) wants to limit the value of the motor torque solutions to the on-line computed maximum and minimum torque applicable according to the wheels speed and provided from the electric motor maps. Negative values of motor torque are meant to be used in regenerative braking, scaled by the vehicle regeneration factor k_{reg}, which in this is set to be unitary.

Finally, opportunely tuning the weights of the optimization function and applying the active set algorithm, the optimal distribution of the torques which minimize the quadratic cost function according to scopes of the implemented torque allocator are obtained.

4 Simulation and results

As already mentioned before, the scope of this thesis work is to evaluate the advantages coming from the integration of the Torque Vectoring developed in the low-level controller of the prototype framework.
Hence, it is necessary to prepare a simulation environment for the suitable testing of the vehicle performances achieved. In the specific case, it has been decided to set-up a Co-Simulation framework exploiting the software Vi-CarRealTime (VI-CRT) capability to be embedded in a MATLAB/Simulink simulation environment.
The VI-CRT is a software offering the possibility to create or import model of vehicle bodies, braking systems, All Wheel Drive (AWD) powertrains, wheels and pneumatics, suspensions and so on.
Thus, it can be used for the creation of very detailed 14 DoF model of a vehicle, allowing the evaluation of the behaviour and performances of a vehicle model in several situation manoeuvres.

This chapter is then dedicated to the presentation of the results obtained from the co-simulation of the MPC and TVC controllers, described in previous sections and implemented in MATLAB/Simulink, and the vehicle the prototype modelled in VI-CRT.

4.1 Co-Simulation Environment

The principal simulation environment is MATLAB/Simulink which make available to the users a VI-CRT's interface, configurable with the input file of the car model, created with the software, to allow the co-simulation. In this way, the whole control system is developed in MATLAB/Simulink, while the VI-CRT is

used to correctly design the vehicle model representing the plant of the control system.

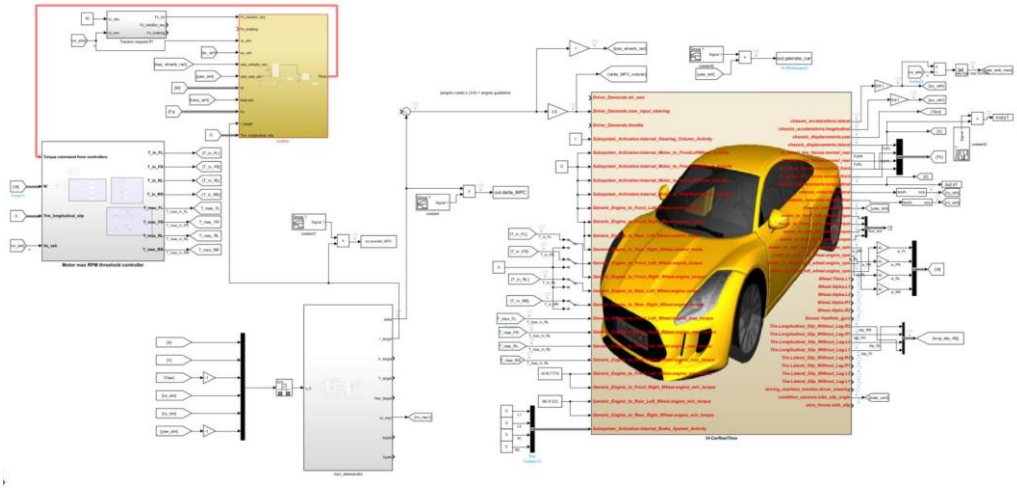

Figure 4.1 – Co-simulation environment with MATLAB/Simulink and VI-CRT

First of all, the VI-CRT interface block is arranged in order to receives as inputs:

- Driver steering command, coming from the MPC due to the autonomous feature of the vehicle.
- Motor torques, coming from the confrontation of the torques output by the TV torque allocator sub-system with the motor maps. This, guaranteeing to receive in input suitable torques according to the current speed of the wheel electric motors.

As for the inputs, the VI-CRT block offers the possibility to extract any needed output signal from the simulation, which represent the feedback signals to obtain a closed-loop control system.
Some of these signals are then used for the graphical representation of the vehicle performances, others as closed-loop feedback.

Concerning the MPC, it receives as input the desired discrete path, generated by a MATLAB script, to be used as a reference for the path tracking. As already mentioned, the MPC contains a linear predictive model used to control the lateral dynamics of the vehicle, for this reason it works assuming a constant longitudinal speed of the vehicle set at $V_{x0} = 10\ m/s$. This value is sufficient valid for considering the dynamic model of the vehicle. The time constant between each iteration of the controller is $T_s = 0.05\ s$. The output of the MPC is a discrete

steering angle signal at the wheels, which is multiplied with the gain 3.6 in order to be transformed into the driver steering command for the VI-CRT plant. This last one passes the current values of the vehicle's states, controlled by the MPC, to guarantee the correct functioning of the predictive model. The needed vehicle's states are the longitudinal and lateral position of the vehicle, the yaw angle, the velocities and the yaw rate.

Moreover, the longitudinal vehicle speed from the VI-CRT plant constitutes a feedback signal also for the PI controller which, differently from the MPC, aims to regulate the longitudinal dynamics of the vehicle.

For what regards the Torque Vectoring, its complete operation in the simulation is explained just as following. The reference generator sub-system is used only for the generation of the vehicle side-slip angle reference β_{ref}, while the yaw rate reference signal comes directly from the MPC as the state evolution.
The TV torque allocator receives as inputs the maximum and minimum suitable torque values from the motor maps according to the motor speed, the additional corrective TV moment M_z and the total torque required T_{req} from the longitudinal controller. To be notice that the torque allocator assigns both positive and negative torques in case respectively of traction or vehicle braking. However, if the electric regenerative braking is not sufficient, the residual braking force is passed to a mechanical braking block to reduce the motor torques as required. In conclusion, the final total torque pilot the plant, entering in the VI-CRT block.

4.2 Simulation Results

Once the co-simulation environment has been set-up, the simulations can be conducted. Specifically, the manoeuvres employed for the evaluation of the MPC and TV controllers are a double lane change and a constant steering. The time of each simulation lasts 15 seconds with a time constant of $T_s = 001\ seconds$.

However, before conducing any simulation manoeuvre, it is necessary to opportunely tune the Internal Model of the controllers, such as the MPC, with the plant model created in VI-CRT. Generally, a typical tuning is done choosing the right values of the cornering stiffness C_f and C_r to have the same understeering behaviour by both the models.

The Figure 4.2 demonstrates that a perfect match between the VI-CRT plant model and the internal vehicle model used in the controllers has been obtained for the values $C_f = 10000\frac{N}{rad}$ and $C_r = 19000\frac{N}{rad}$.

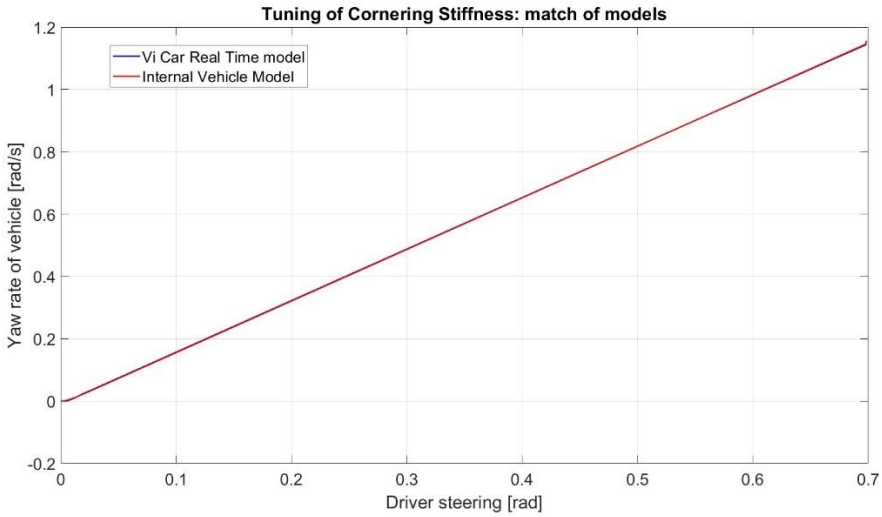

Figure 4.2 – Cornering stiffness comparison between Vi CRT plant model (blue line) And MPC internal vehicle model (red line) without model mismatch. Cornering stiffness values used are $C_f = 10000\ N/rad$ and $C_r = 19000\ N/rad$.

In the following paragraph the results of the simulations are presented, highlighting the differences respectively due to the passive TV and its activation.

Moreover, the results of simulations with new values of cornering stiffness, $C_f = 25000\frac{N}{rad}$ and $C_r = 30000\frac{N}{rad}$, are reported too with the scope of furtherly highlight the advantages of the TV in the mitigation of eventual presence of Plant model mismatch. In fact, errors due to linearization of the model or due parameters not sufficient accurately estimated could lead to a mismatch between the internal vehicle model and the one used in the plant.

As demonstrated by the Figure 4.3, a Plant model mismatch reveals as instance a not equal understeering behaviours from the two models, meaning that different vehicle's yaw rate values correspond to the same steering angle value. In particular, the MPC internal model reveals a less understeering behaviour.

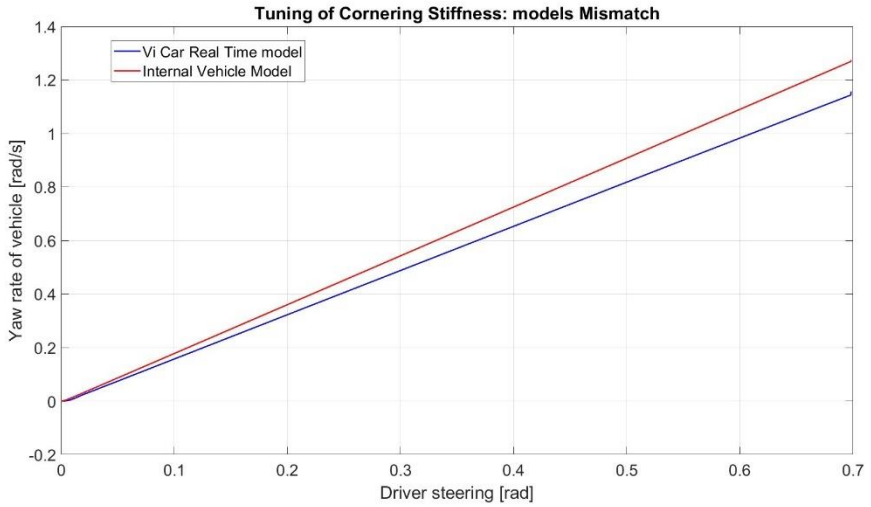

Figure 4.3 – Cornering stiffness comparison between Vi CRT plant model (blue line) And MPC internal vehicle model (red line) with voluntary model mismatch. Cornering stiffness values used are $C_f = 25000\ N/rad$ and $C_r = 30000\ N/rad$.

4.2.1 Double lane change manoeuvre

The first manoeuvre is a double lane change. The following results aims to evidence the ability of the vehicle control system to perform path tracking, comparing also the cross-track errors obtained. Moreover, graphical representations of the motor torques, steering angle and yaw rate of the vehicle are shown, followed by some considerations on the results obtained.

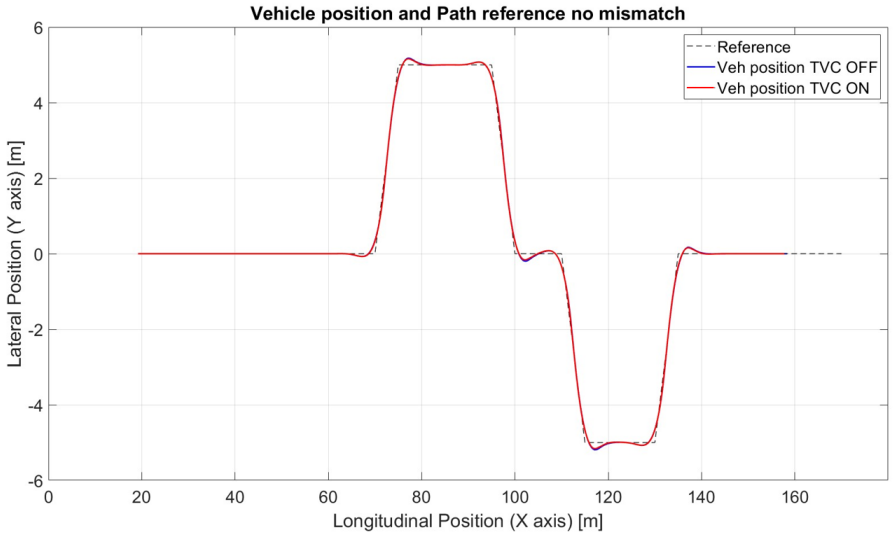

Figure 4.4 – Vehicle position on the XY plane in the case of TVC OFF (blue line) and TVC ON (red line) w.r.t. the reference trajectory (dotted line) with cornering stiffness values $C_f = 10000\ N/rad$ and $C_r = 19000\ N/rad$.

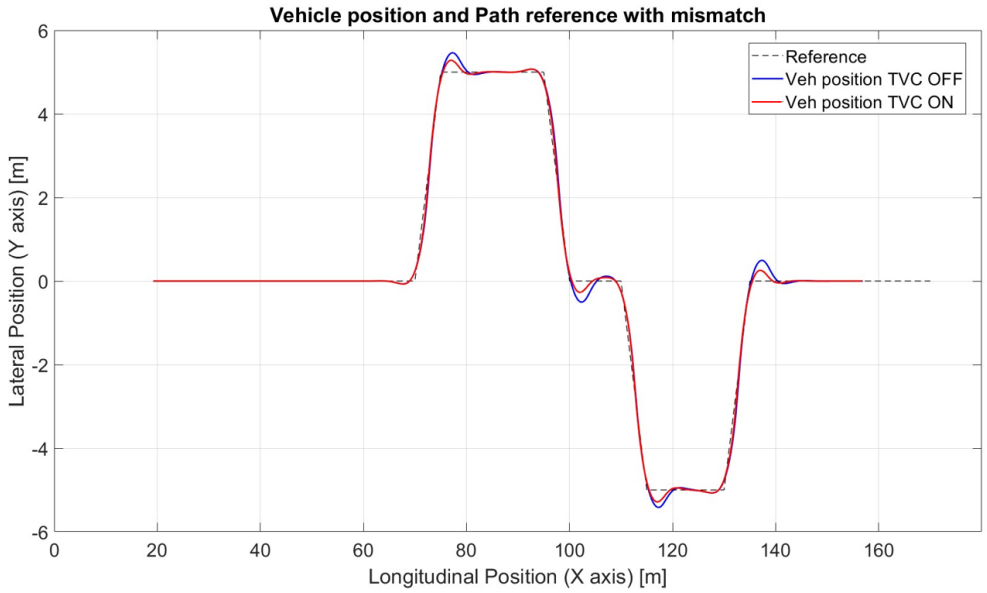

Figure 4.5 – Vehicle position on the XY plane in the case of TVC OFF (blue line) and TVC ON (red line) w.r.t. the reference trajectory (dotted line) with cornering stiffness values $C_f = 25000\ N/rad$ and $C_r = 30000\ N/rad$.

In the Figure 4.4, it is possible to notice that the difference between the case with TV deactivated (TVC OFF, blue line) and the case with TV controller activation (TVC ON, red line) is very slightly. In fact, the MPC succeeds in the path tracking of the reference path, reported with a black dotted line, quite well. This is due to the perfect match between the predictive model and the VI-CRT model in the plant, as already explained. Hence, the effect of the Torque Vectoring is limited by the optimal control of the vehicle lateral dynamics performed by the MPC.

On the contrary, the case with Plant model mismatch in Figure 4.5 shows the positive effect of the activation of the TV controller. In other words, the TVC acts correcting the mismatch due to the missing tuning of the predictive model and forces the plant behaving closely to the MPC internal model, traduced in a model following action by the TVC.

In support to the considerations done above, the Figure 4.6 and Figure 4.7 report the cross-track errors comparing the values obtained with TV deactivated and activated, both in the case of model match and in the case of plant model mismatch.

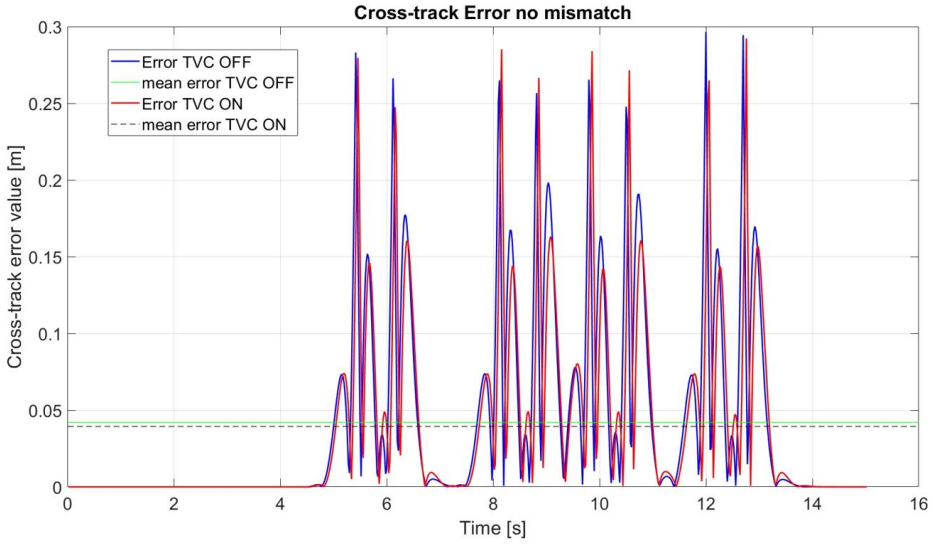

Figure 4.6 – Cross-track error between the vehicle position and the reference trajectory in the case of TVC OFF (blue line) and TVC ON (red line). Mean errors are in green line for TVC OFF and in black dotted line for TVC ON, with cornering stiffness values $C_f = 10000\ N/rad$ and $C_r = 19000\ N/rad$.

In the Figure 4.6 the cross-track error in the case of TVC OFF reaches lower values than the case of TVC OFF with Plant model mismatch, due to the optimal estimations from the MPC. However, the lines in red reporting the results in the case of TV activation demonstrated in both the two figures similar values of cross-track error, which are both lower than 0,3 m.

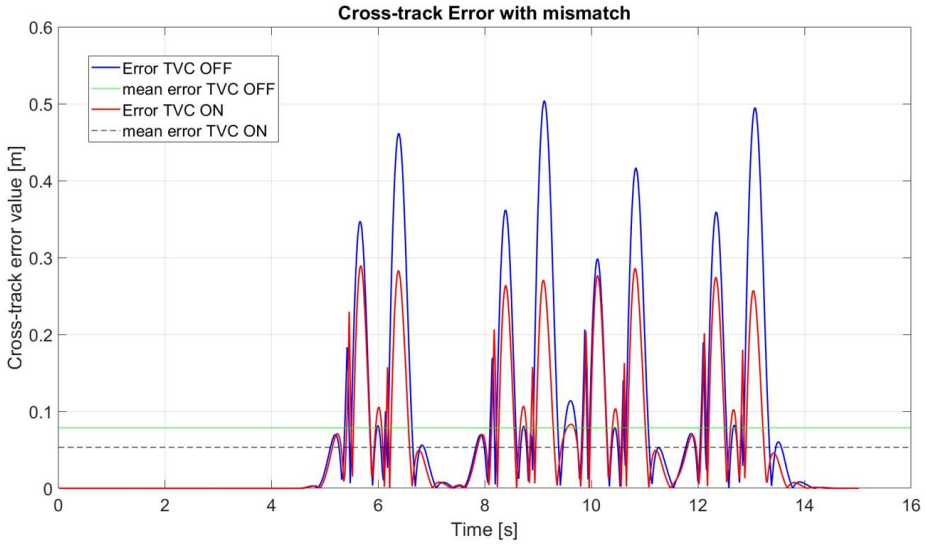

Figure 4.7 – Cross-track error between the vehicle position and the reference trajectory in the case of TVC OFF (blue line) and TVC ON (red line). Mean errors are in green line for TVC

OFF and in black dotted line for TVC ON, with cornering stiffness values $C_f = 20000\ N/rad$ and $C_r = 35000\ N/rad$.

Additionally, the Mean Absolute of the cross-track errors are summed up in Table 1, where it can be noticed that while in the case of model match the effect of TVC in the reduction of the cross-track error mean is slightly, in the other case is much more evident.

	Cross-track error Mean Absolute (m)	
	Model match	**Plant model mismatch**
TVC OFF	0.0418	0.0790
TVC ON	0.0392	0.0536

Table 1 – Mean Absolute of the cross-track errors.

Hence, this is a confirmation of the contribute by the Torque Vectoring controller in the improving of the MPC functioning.

The Figure 4.8 and Figure 4.9 exhibit more in deep the action of the TV in the generation of the additional moment M_z, by the state-space feedback in the high level of the TVC, and its distribution on the four wheels by the torque allocator. Even if the peaks are quite pronounced, it should be reminded that the torque will be actuated according to the motor characteristics, limiting the risk of aggressive action.

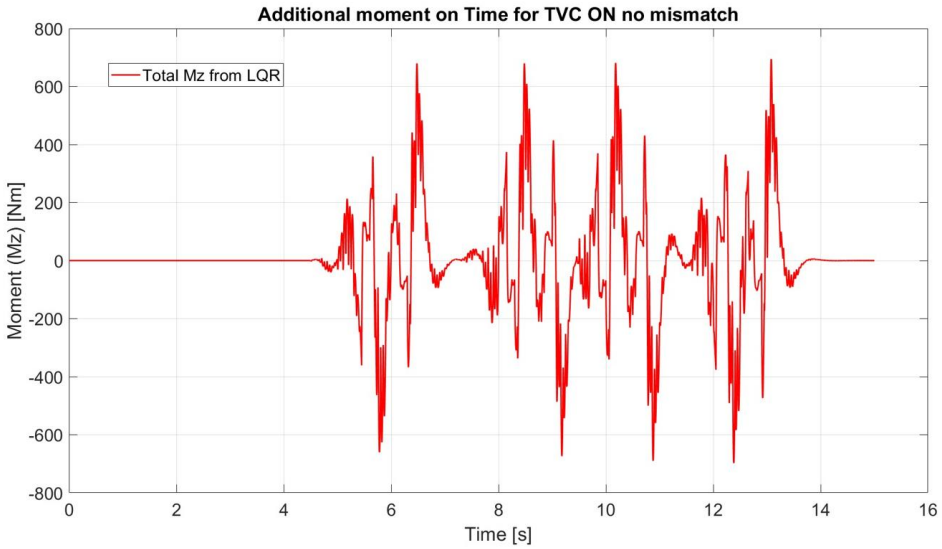

Figure 4.8 – Additional corrective moment M_z coming from the TV high-level block with cornering stiffness values $C_f = 10000\ N/rad$ and $C_r = 19000\ N/rad$.

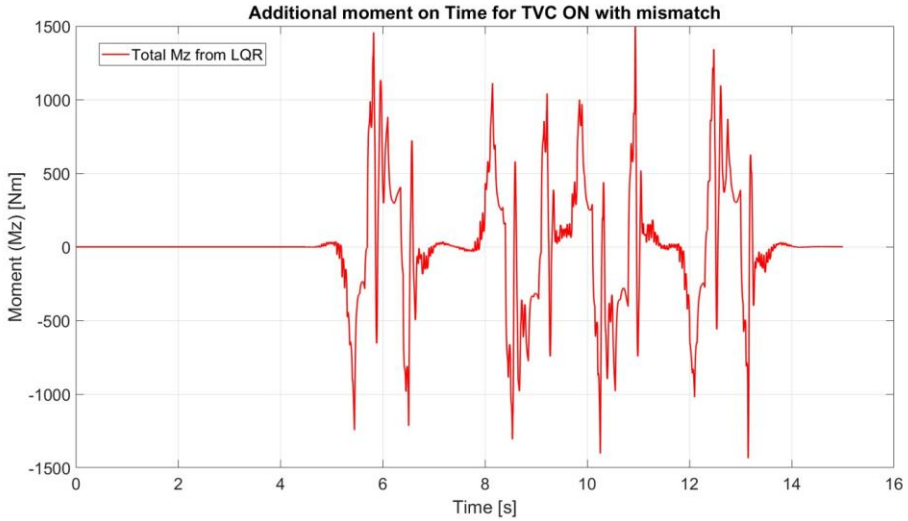

Figure 4.9 – Additional corrective moment M_z coming from the TV high-level block with cornering stiffness values $C_f = 25000\ N/rad$ and $C_r = 30000\ N/rad$.

In the Figure 4.10 and Figure 4.12 the motor torques are the same on the four wheel, with a slightly higher values of the rear motor torques with respect to the front ones. In fact, in the case of passive TV the torque allocator distributes a few torque portion more on the rear wheels in order to increase the vehicle's stability. Instead, Figure 4.11 and Figure 4.13 show the motor torque distribution due to the applying the additional corrective moment M_z.

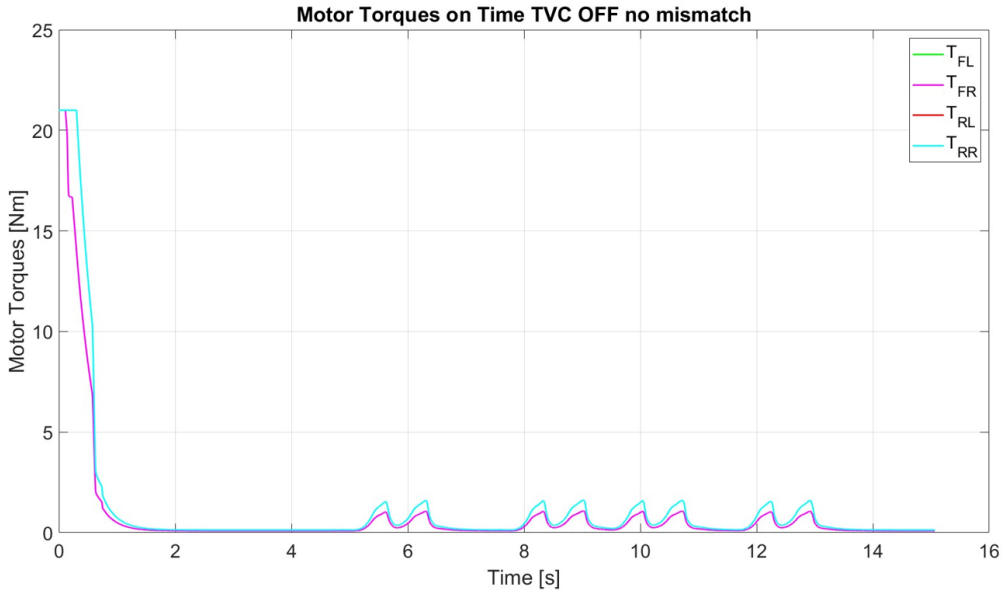

Figure 4.10 – Motor torques distribution on the four wheels with TVC OFF with cornering stiffness values $C_f = 10000\ N/rad$ and $C_r = 19000\ N/rad$.

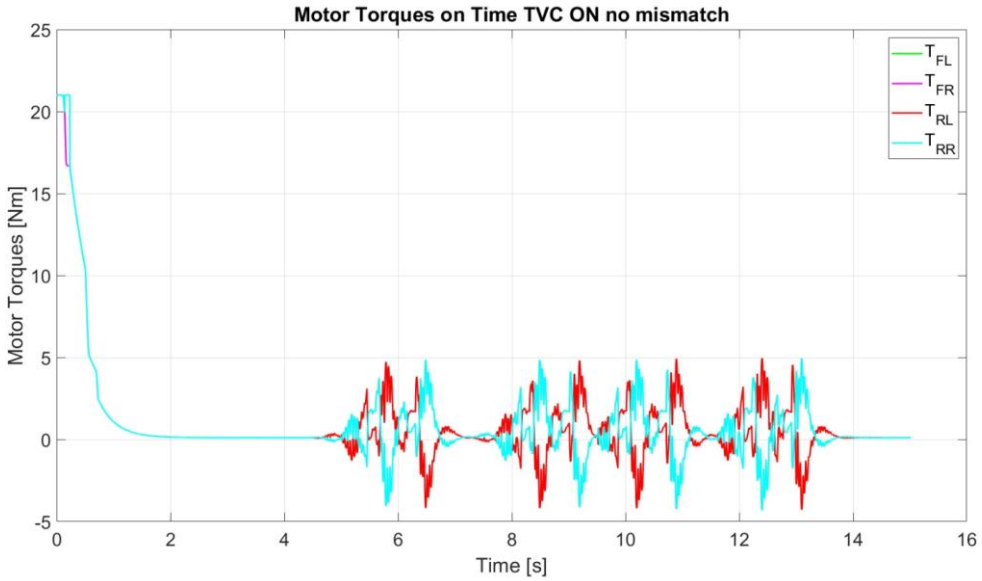

Figure 4.11 – Motor torques distribution on the four wheels with TVC ON with cornering stiffness values $C_f = 10000\ N/rad$ and $C_r = 19000\ N/rad$.

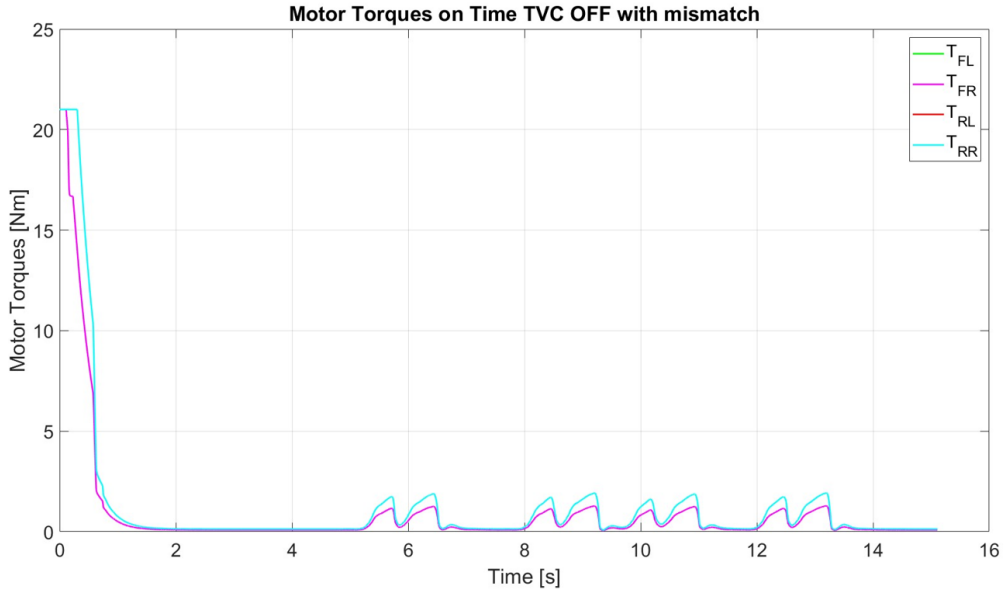

Figure 4.12 – Motor torques distribution on the four wheels with TVC OFF with cornering stiffness values $C_f = 25000\ N/rad$ and $C_r = 30000\ N/rad$.

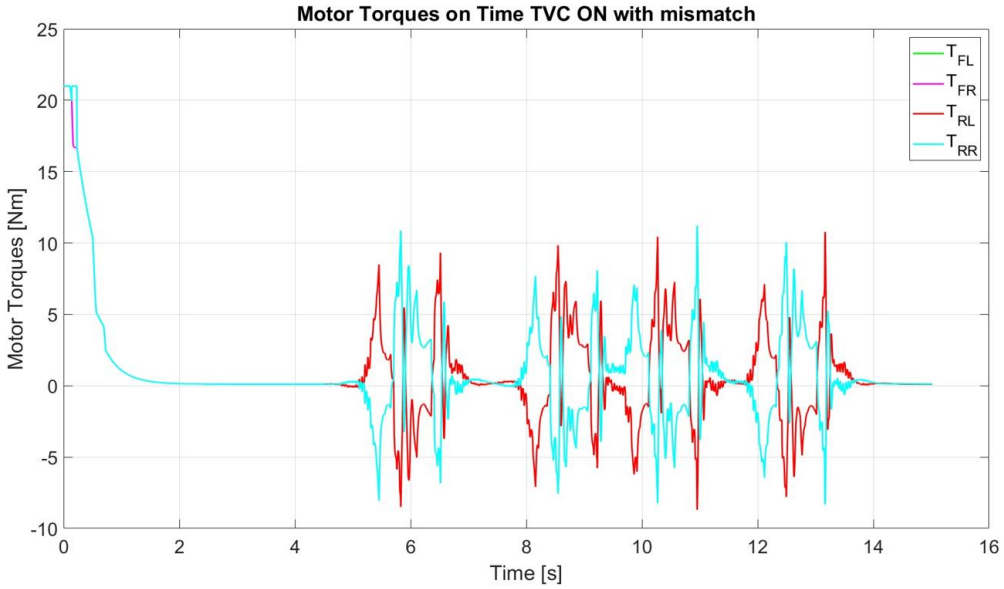

Figure 4.13 – Motor torques distribution on the four wheels with TVC ON with cornering stiffness values $C_f = 25000\ N/rad$ and $C_r = 30000\ N/rad$.

In the Figure 4.14 and Figure 4.15 the steering angles at the wheels coming from the MPC are shown. In particular, in the first one it is possible to notice a very similar steering action in the cases of passive and active TVC due to the correct MPC prediction. Instead, in the other one it is evident that the advantages of the TVC activation are mainly in the anticipation of the steering action and in the reduction of the steering effort.

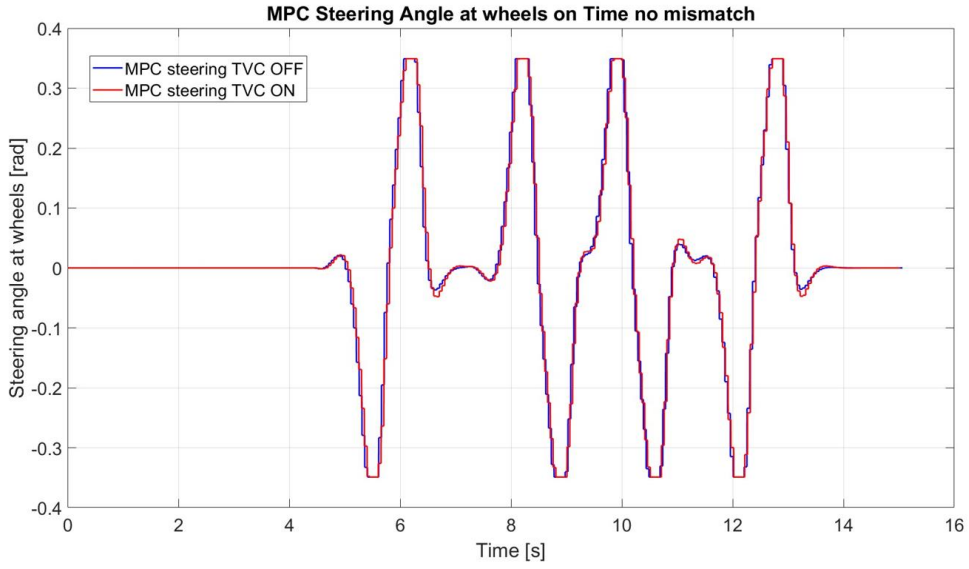

Figure 4.14 – Optimal predicted steering angle in the case of TVC OFF (blue line) and TVC ON (red line) with cornering stiffness values $C_f = 10000\ N/rad$ and $C_r = 19000\ N/rad$.

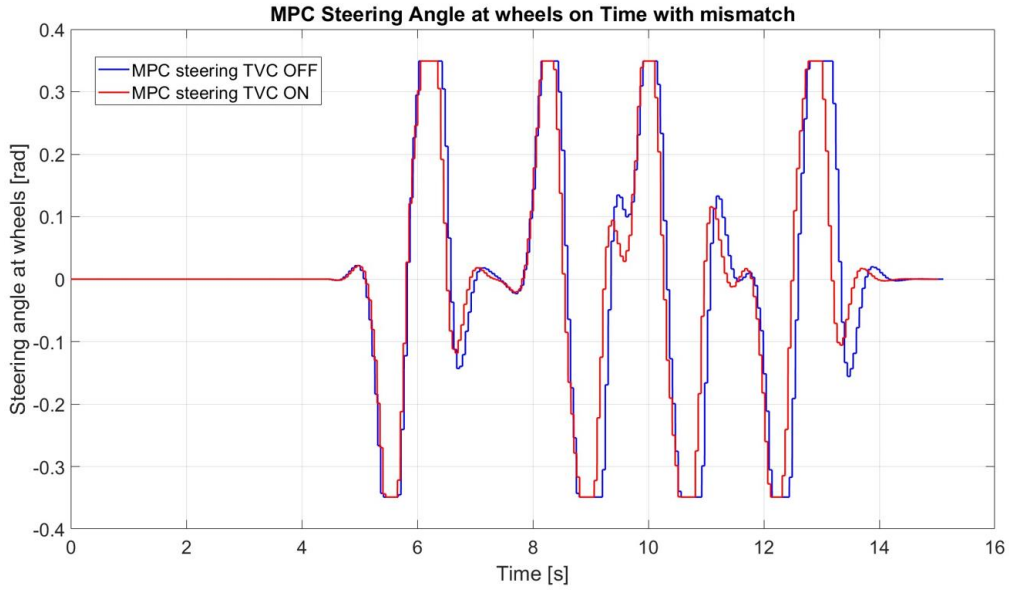

Figure 4.15 – Optimal predicted steering angle in the case of TVC OFF (blue line) and TVC ON (red line) with cornering stiffness values $C_f = 25000\ N/rad$ and $C_r = 30000\ N/rad$.

The Mean Absolute of the steering angle at the wheels and the percentage of reduction of the mean in the case of TVC ON with respect to the one of the TVC OFF are reassumed.

Steering angle at wheels				
	Mean Absolute (rad)		Percentage of reduction TVC ON w.r.t TVC OFF	
	Model match	Plant model mismatch	Model match	Plant model mismatch
TVC OFF	0.0888	0.1108	-	-
TVC ON	0.0887	0.0958	-0.1%	-13.54%

Table 2 – Mean Absolute and percentage of reduction of the steering angle at wheels

Concerning the vehicle yaw rates, the Figure 4.16 again doesn't evidence important differences. However, in the case of Plant model mismatch in Figure 4.17, the comparison of the blue line (TVC OFF) with the red one (TVC ON) confirms the same positive effects already seen for the steering angle at wheels due to the activation of the TVC.

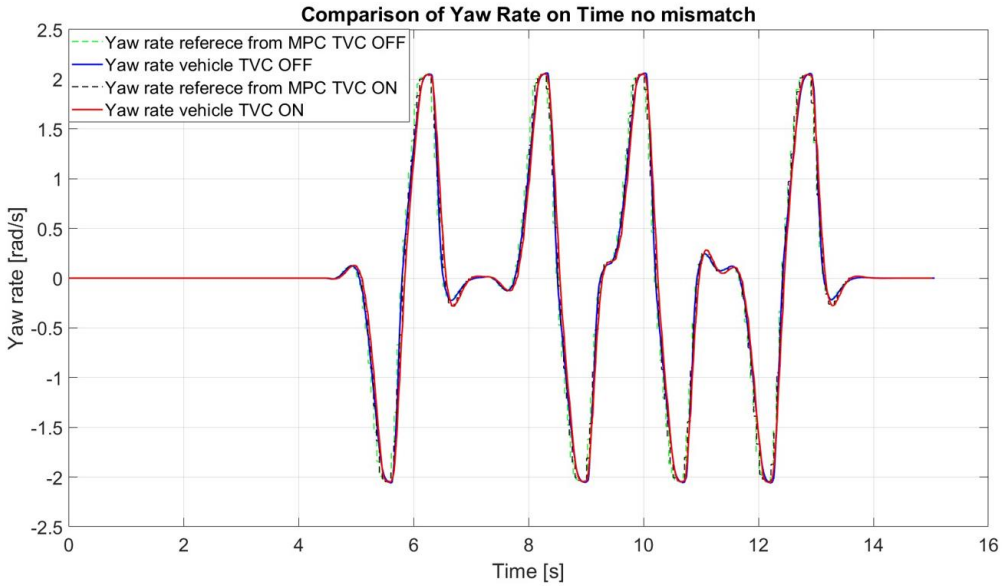

Figure 4.16 – Vehicle yaw rate in the case of TVC OFF (blue line) following the predicted yaw rate reference (green dotted line) w.r.t the vehicle yaw rate in case of TVC ON (red line) following the yaw rate reference (black dotted line) with cornering stiffness values $C_f = 10000\ N/rad$ and $C_r = 19000\ N/rad$.

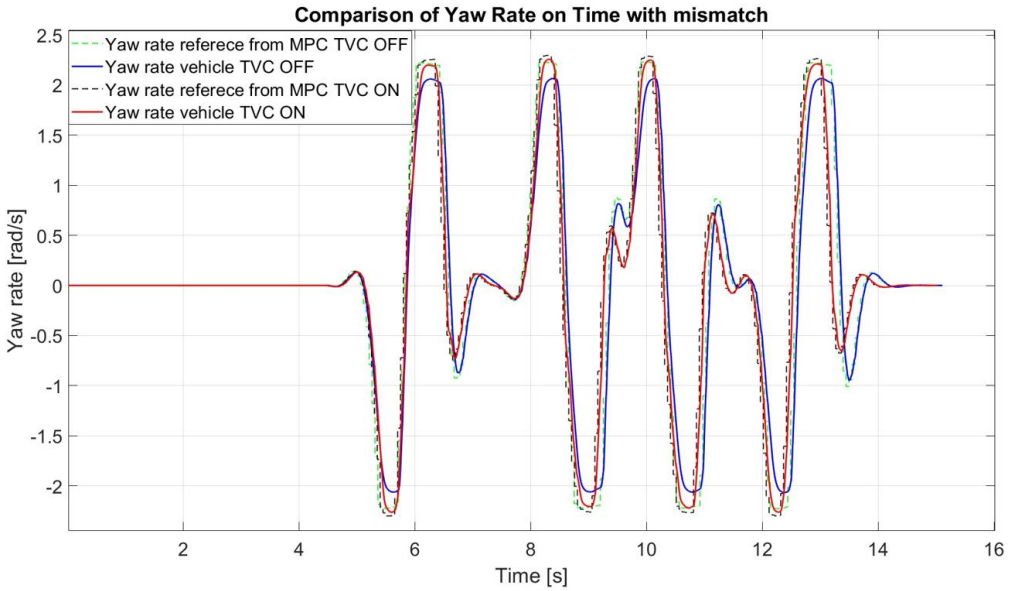

Figure 4.17 – Vehicle yaw rate in the case of TVC OFF (blue line) following the predicted yaw rate reference (green dotted line) w.r.t the vehicle yaw rate in case of TVC ON (red line) following the yaw rate reference (black dotted line) with cornering stiffness values $C_f = 25000\ N/rad$ and $C_r = 30000\ N/rad$.

Moreover, the actual vehicle's yaw rate in the case of TVC ON follows better the yaw rate reference (black line) coming from the MPC, especially in correspondence of the yaw rates peaks. This important result points out that the TVC helps the vehicle model better following the yaw rate reference predicted by the MPC.

The deviations of the vehicle's yaw rates with respect to the yaw rate references exhibit a general reduction of the peaks due to the Torque Vectoring in Figure 4.18 and Figure 4.19. While numerical values and the percentage of yaw rate deviation in the cases of TVC OFF and OFF and in the case of model match and plant model mismatch are reported in Table 3.

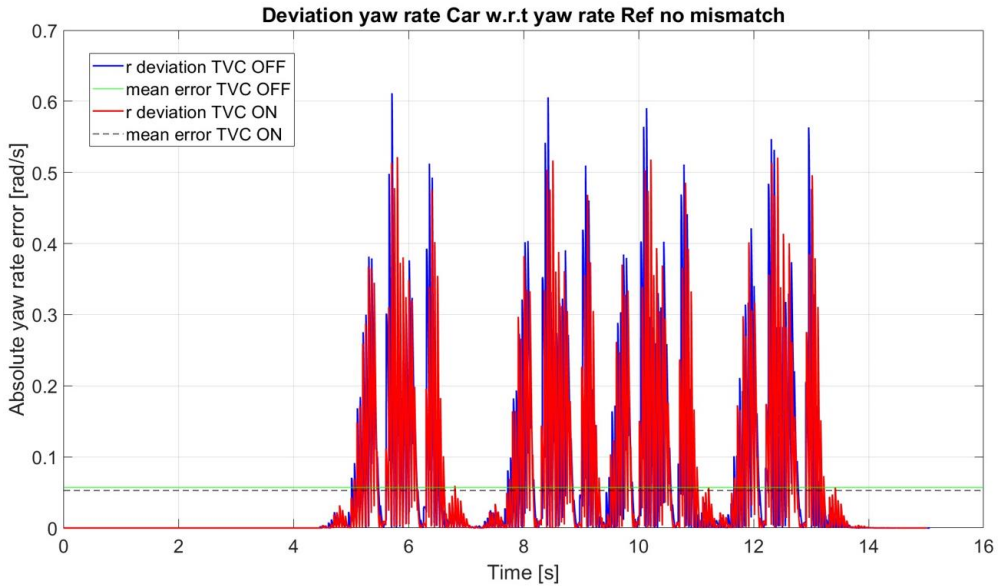

Figure 4.18 – Vehicle yaw rate deviation w.r.t to predicted yaw rate in case of TVC OFF (blue line) and TVC ON (red line). Mean errors are in green line for TVC OFF and in black dotted line for TVC ON, with cornering stiffness values $C_f = 10000\ N/rad$ and $C_r = 19000\ N/rad$.

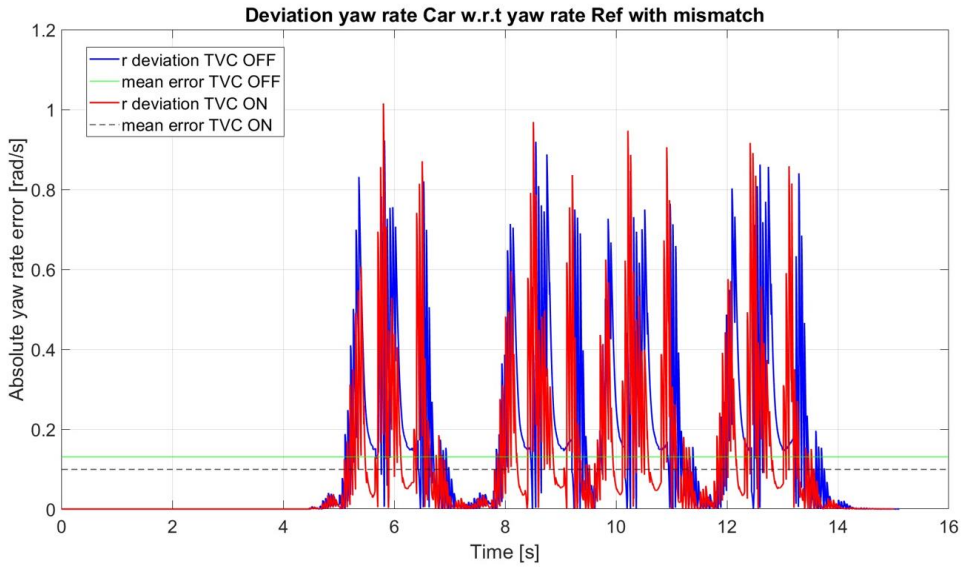

Figure 4.19 – Vehicle yaw rate deviation w.r.t to predicted yaw rate in case of TVC OFF (blue line) and TVC ON (red line). Mean errors are in green line for TVC OFF and in black dotted line for TVC ON, with cornering stiffness values $C_f = 25000\ N/rad$ and $C_r = 30000\ N/rad$.

Deviation of current vehicle's yaw rate w.r.t yaw rate reference				
	Mean Absolute Error (rad/s)		**Percentage of reduction w.r.t TVC OFF**	
	Model match	**Plant model mismatch**	**Model match**	**Plant model mismatch**
TVC OFF	0.0568	0.1299	-	-
TVC ON	0.0531	0.0992	-6.51%	-23.63%

Table 3 – Deviation of the vehicle yaw rate w.r.t the yaw rate reference

4.2.2 Constant steering manoeuvre

The second manoeuvre consists in the vehicle dealing with a circumference of constant radius, hence in a constant steering situation.

The same presentation procedure of the double lane change has been adopted also in this case.

In particular, in Figure 4.20 and Figure 4.21 it can be noticed that the when the vehicle start from the initial position, the path tracking is not perfectly satisfied. This is due to the vehicle acceleration for reaching the reference speed. Thus,

during this transient, the effects of the TVC activation are more evident in both the cases of match and mismatch of the model. In fact, the lateral MPC has been implemented to consider the longitudinal speed of the car constant.

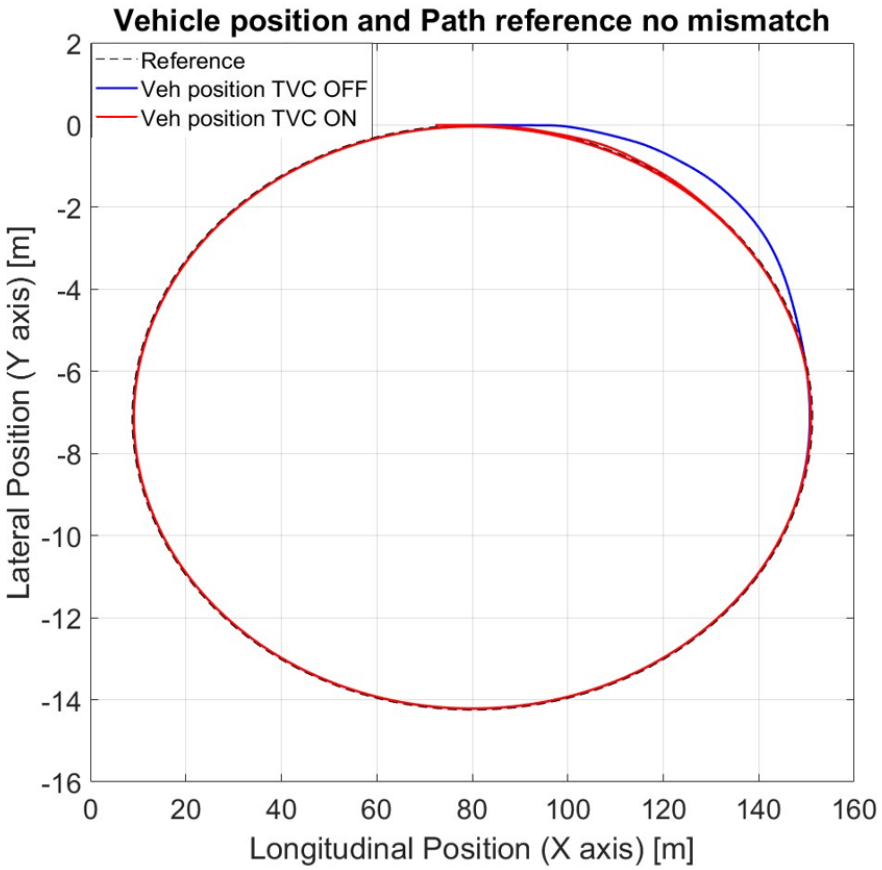

Figure 4.20 – Vehicle position on the XY plane in the case of TVC OFF (blue line) and TVC ON (red line) w.r.t. the reference trajectory (dotted line) with cornering stiffness values $C_f = 10000\ N/rad$ and $C_r = 19000\ N/rad$.

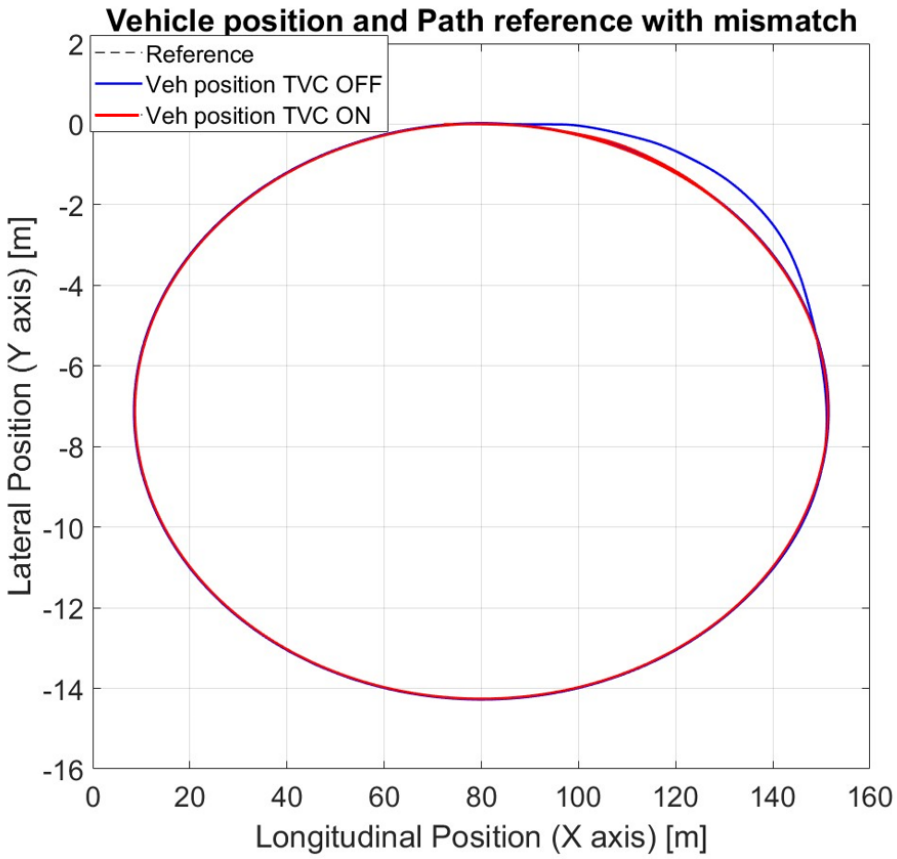

Figure 4.21 – Vehicle position on the XY plane in the case of TVC OFF (blue line) and TVC ON (red line) w.r.t. the reference trajectory (dotted line) with cornering stiffness values $C_f = 25000\ N/rad$ and $C_r = 30000\ N/rad$.

The graphics of the cross-track error (Figure 4.22 and Figure 4.23) exhibit a peak in correspondence of the transient in the case of TVC OFF, as already explained above. However, these errors are mitigated efficiently by the activation of the Torque Vectoring, pointing out a significant contribution of the TVC in the path tracking. Thus, the advantage of using the TV is having a vehicle behaviour closer to the predictions of the MPC, which at the same time result also more reliable.

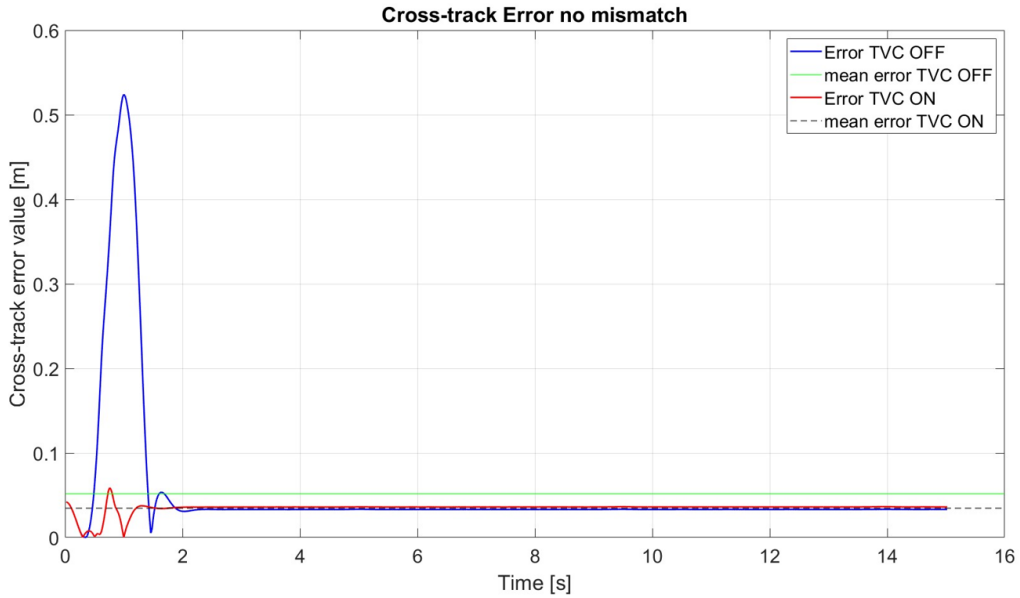

Figure 4.22 – Cross-track error between the vehicle position and the reference trajectory in the case of TVC OFF (blue line) and TVC ON (red line). Mean errors are in green line for TVC OFF and in black dotted line for TVC ON, with cornering stiffness values $C_f = 10000\ N/rad$ and $C_r = 19000\ N/rad$.

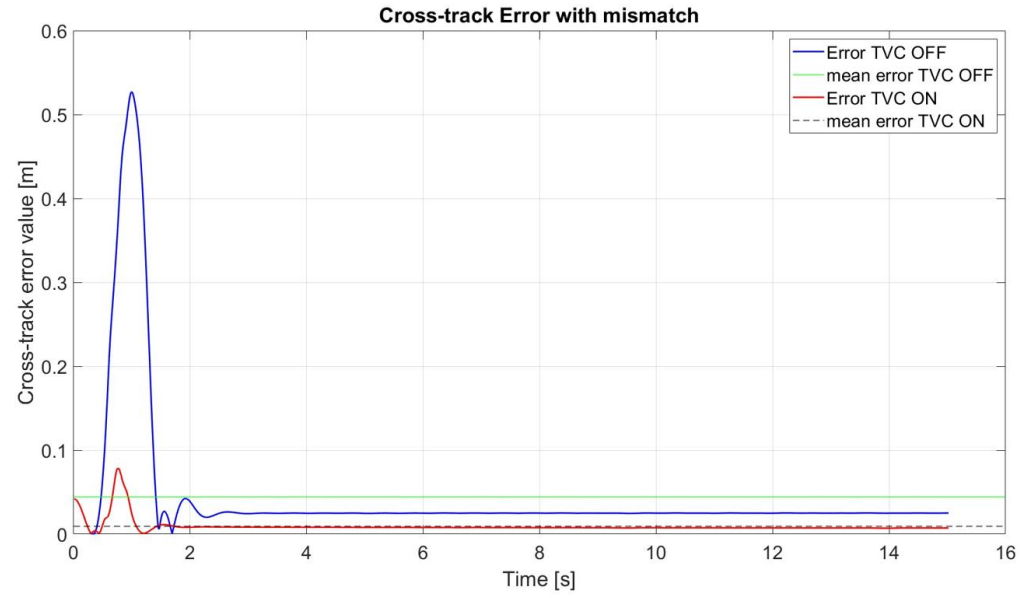

Figure 4.23 – Cross-track error between the vehicle position and the reference trajectory in the case of TVC OFF (blue line) and TVC ON (red line). Mean errors are in green line for TVC OFF and in black dotted line for TVC ON, with cornering stiffness values $C_f = 25000\ N/rad$ and $C_r = 30000\ N/rad$.

Values of the Means Absolute of the cross-track errors are reported in the Table 4, aiming to numerically confirm the results clearly evident by the Figure 4.22 and Figure 4.23.

	Cross-track error Mean Absolute (m)	
	Model match	**Plant model mismatch**
TVC OFF	0.0516	0.0441
TVC ON	0.0350	0.0094

Table 4 – Mean Absolute of the cross-track error in second manoeuvre

Then, Figure 4.24 and Figure 4.25 represent the additional moment M_z generated by the Torque Vectoring, while from Figure 4.26 to Figure 4.29 the effects of the additional moment application on the motor torques distribution is are showned also for this manoeuvre.

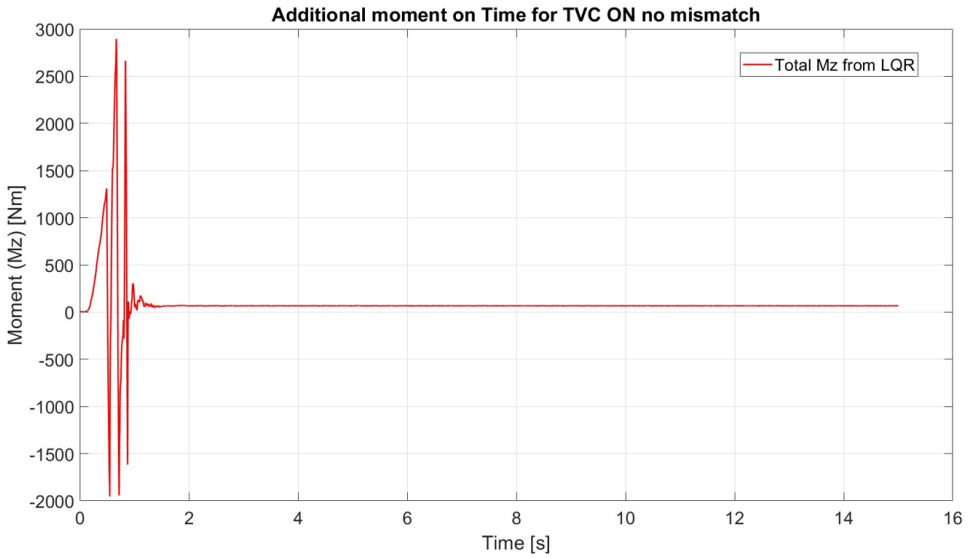

Figure 4.24 – Additional corrective moment M_z coming from the TV high-level block with cornering stiffness values $C_f = 10000\ N/rad$ and $C_r = 19000\ N/rad$.

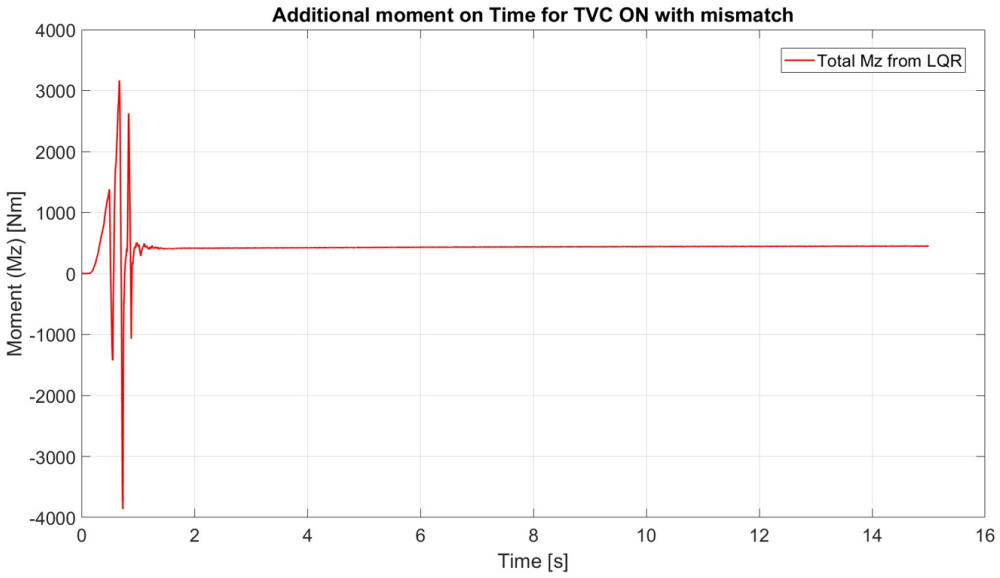

Figure 4.25 – Additional corrective moment M_z coming from the TV high-level block with cornering stiffness values $C_f = 25000\ N/rad$ and $C_r = 30000\ N/rad$.

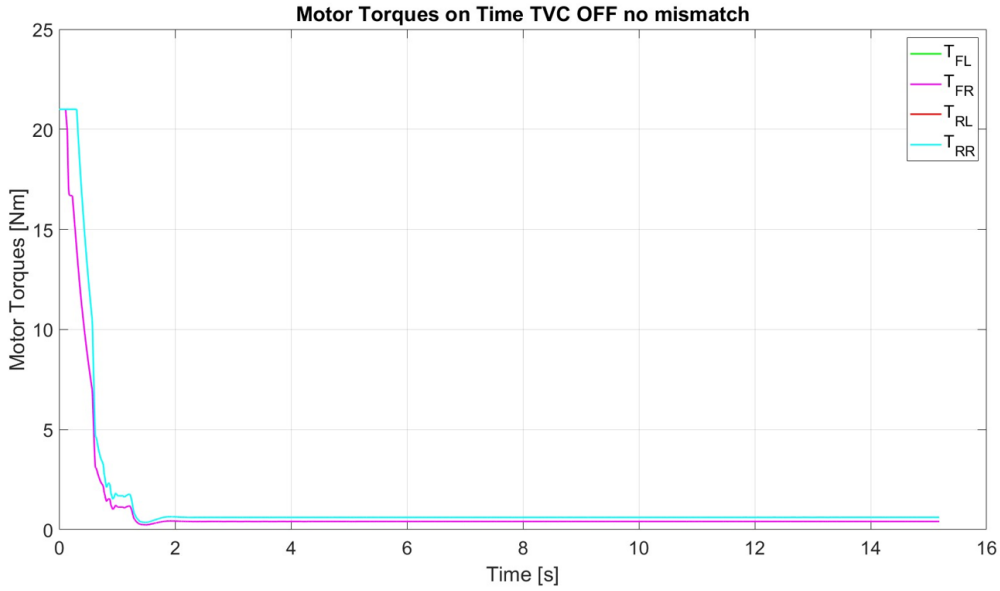

Figure 4.26 – Motor torques distribution on the four wheels with TVC OFF with cornering stiffness values $C_f = 10000\ N/rad$ and $C_r = 19000\ N/rad$.

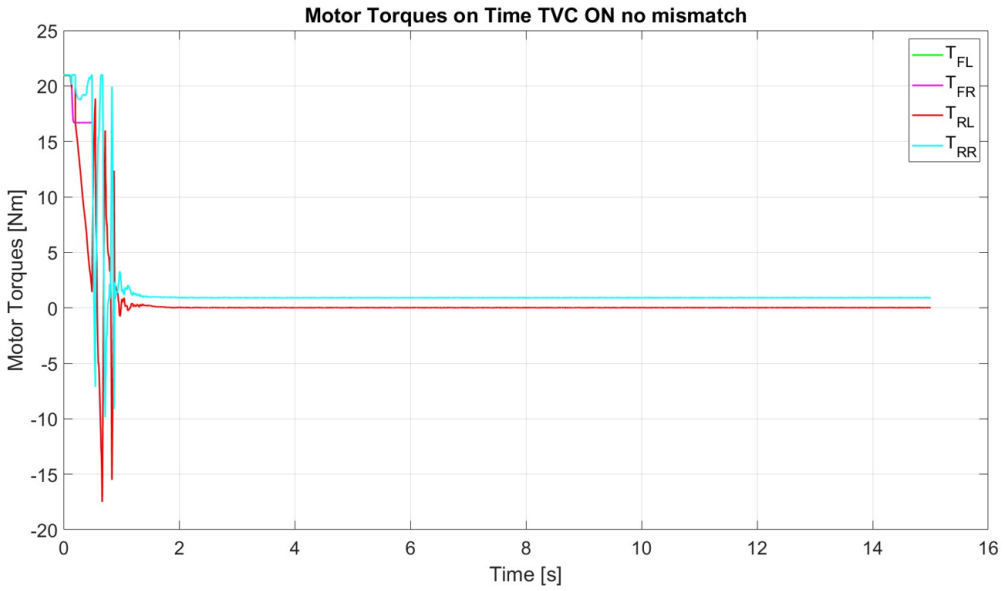

Figure 4.27 – Motor torques distribution on the four wheels with TVC ON with cornering stiffness values $C_f = 10000\ N/rad$ and $C_r = 19000\ N/rad$.

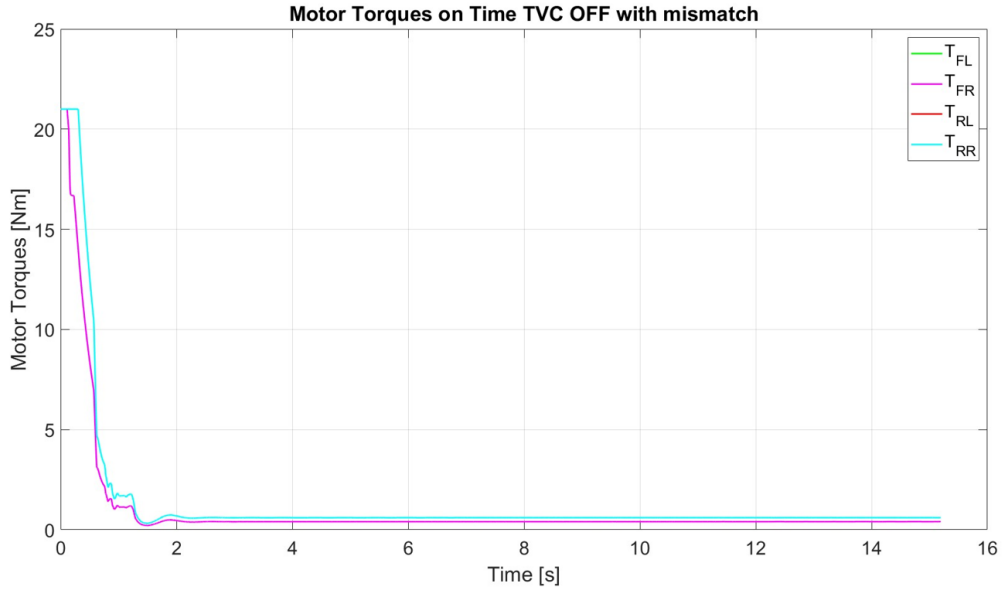

Figure 4.28 – Motor torques distribution on the four wheels with TVC OFF with cornering stiffness values $C_f = 25000\ N/rad$ and $C_r = 30000\ N/rad$.

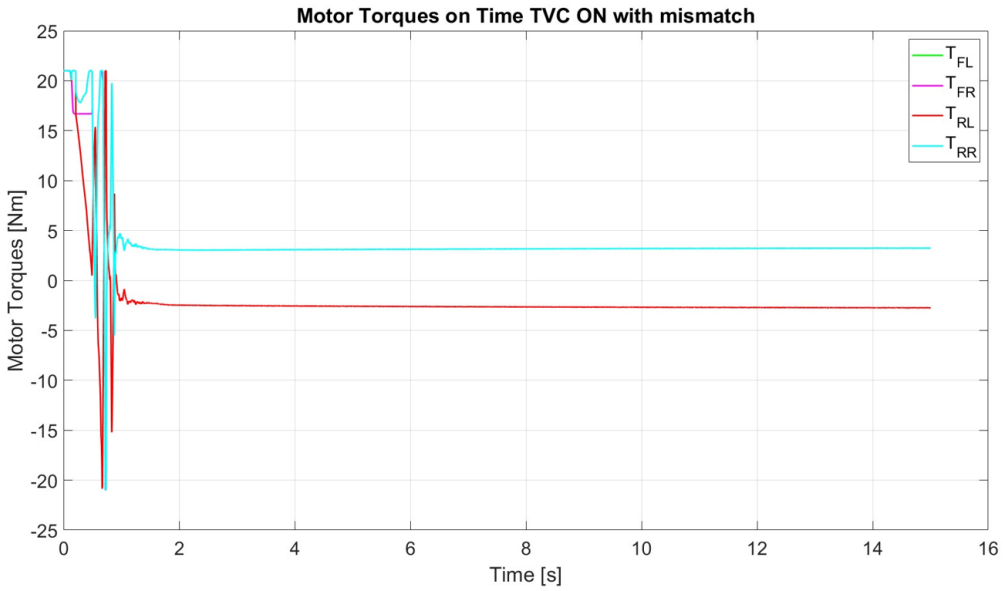

Figure 4.29 – Motor torques distribution on the four wheels with TVC ON with cornering stiffness values $C_f = 25000\ N/rad$ and $C_r = 30000\ N/rad$.

Finally, the steering angle and yaw rate graphics both confirm the results achieved up to now.

Concerning the steering angle in Figure 4.30, the presence of the TVC reduces the transient both in duration and amplitude. Hence, the Figure 4.30 points out how the TV contributes into the anticipation of the transient reduction and the reduction of the total steering effort.

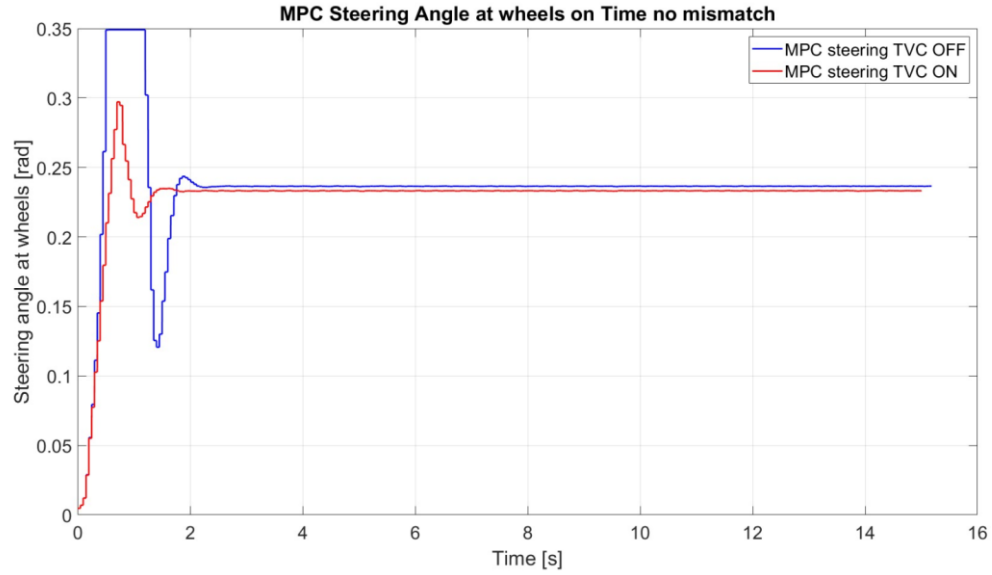

Figure 4.30 – Optimal predicted steering angle in the case of TVC OFF (blue line) and TVC ON (red line) with cornering stiffness values $C_f = 10000\ N/rad$ and $C_r = 19000\ N/rad$.

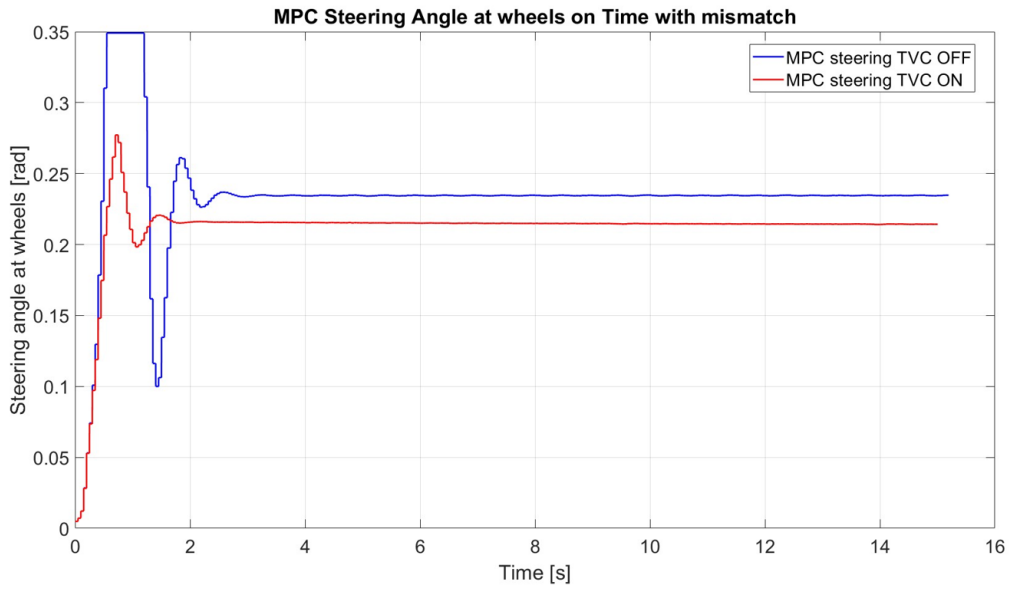

Figure 4.31 – Optimal predicted steering angle in the case of TVC OFF (blue line) and TVC ON (red line) with cornering stiffness values $C_f = 25000\ N/rad$ and $C_r = 30000\ N/rad$.

The numerical values showing the reduction of the steering effort are collected in Table 5.

Steering angle at wheels				
	Mean Absolute (rad)		**Percentage of reduction of the TVC ON w.r.t TVC OFF**	
	Model match	**Plant model mismatch**	**Model match**	**Plant model mismatch**
TVC OFF	0.2351	0.2330	-	-
TVC ON	0.2284	0.2109	-2.85%	-9.48%

Table 5 – Mean Absolute and percentage of reduction of the steering angle at wheels

For what regards the yaw rate, same considerations already done for the double lane change manoeuvre are valid. In fact, the TVC helps the MPC in the path tracking, making the current yaw rate state of the car following better the reference coming from the MPC both in transient and in steady state, as showed in Figure 4.32 and Figure 4.33. The differences of the yaw rate references between the case of perfect match and mismatch of the models are due to the dependence of the yaw rate reference to the steering angle.

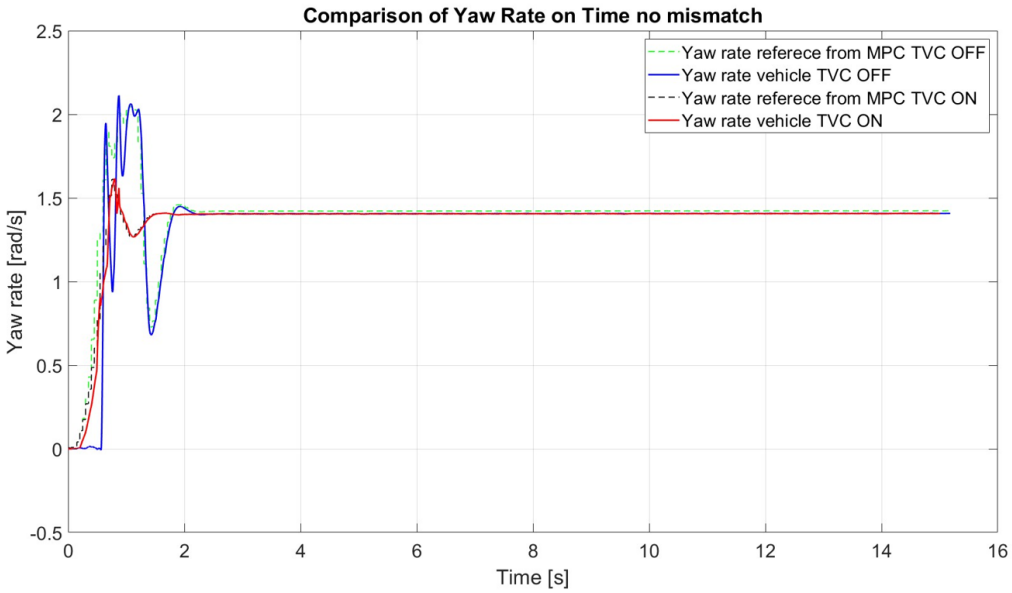

Figure 4.32 – Vehicle yaw rate in the case of TVC OFF (blue line) following the predicted yaw rate reference (green dotted line) w.r.t the vehicle yaw rate in case of TVC ON (red line) following the yaw rate reference (black dotted line) with cornering stiffness values $C_f = 10000\ N/rad$ and $C_r = 19000\ N/rad$.

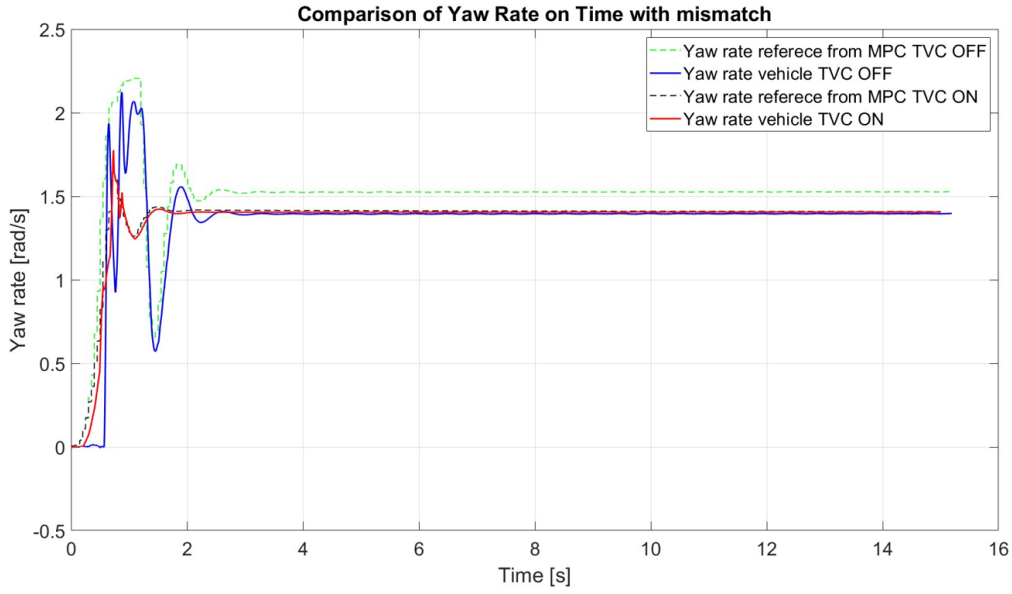

Figure 4.33 – Vehicle yaw rate in the case of TVC OFF (blue line) following the predicted yaw rate reference (green dotted line) w.r.t the vehicle yaw rate in case of TVC ON (red line) following the yaw rate reference (black dotted line) with cornering stiffness values $C_f = 25000\ N/rad$ and $C_r = 30000\ N/rad$.

As further confirmation, the deviations of the vehicle's yaw rate respect to the yaw rate reference are shown both graphically in Figure 4.34 and Figure 4.35 and numerically in Table 6.

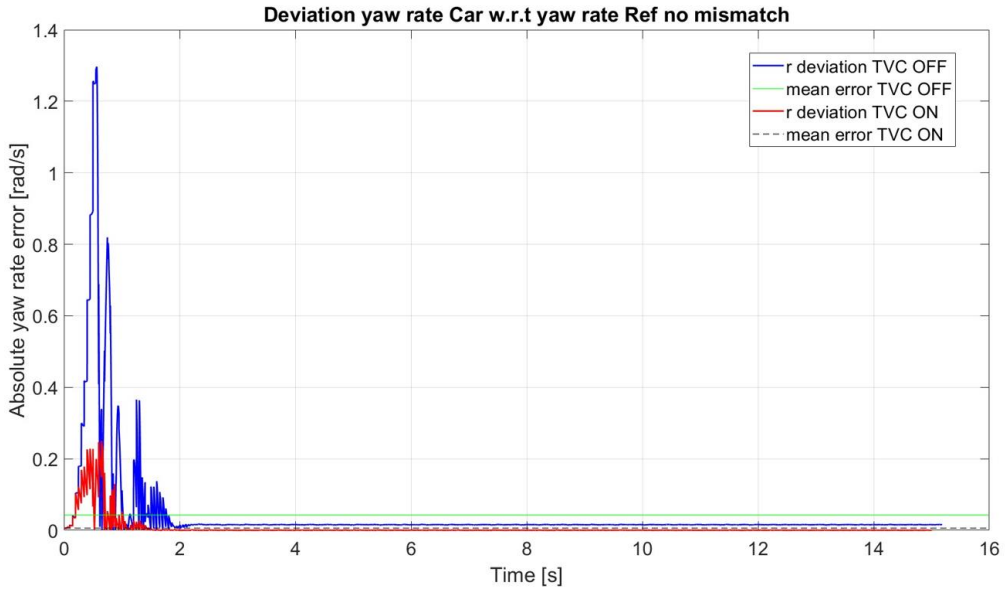

Figure 4.34 – Vehicle yaw rate deviation w.r.t to predicted yaw rate in case of TVC OFF (blue line) and TVC ON (red line). Mean errors are in green line for TVC OFF and in black dotted line for TVC ON, with cornering stiffness values $C_f = 10000\ N/rad$ and $C_r = 19000\ N/rad$.

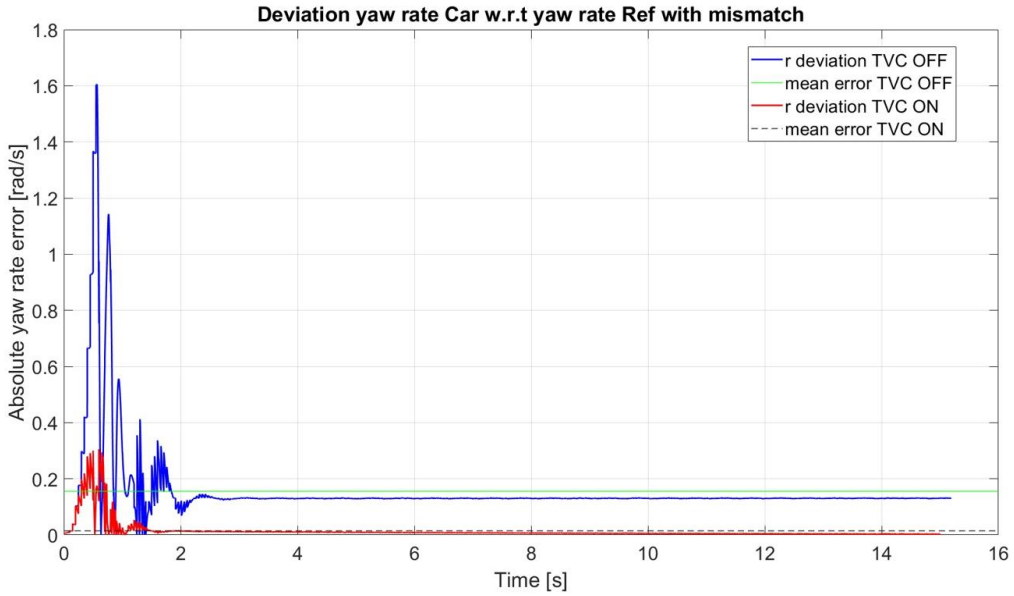

Figure 4.35 – Vehicle yaw rate deviation w.r.t to predicted yaw rate in case of TVC OFF (blue line) and TVC ON (red line). Mean errors are in green line for TVC OFF and in black dotted line for TVC ON, with cornering stiffness values $C_f = 25000\ N/rad$ and $C_r = 30000\ N/rad$.

Deviation of current vehicle's yaw rate w.r.t yaw rate reference				
	Mean Absolute Error (rad/s)		**Percentage of reduction w.r.t TVC OFF**	
	Model match	**Plant model mismatch**	**Model match**	**Plant model mismatch**
TVC OFF	0.0423	0.1547	-	-
TVC ON	0.0062	0.0139	-85.34%	-91.01%

Table 6 – Deviation of the vehicle yaw rate w.r.t the yaw rate reference

Conclusions

Results

The aim of this thesis has been the designing of a Torque Vectoring control strategy to the improve the robustness of the MPC integrated in the low-level control of the SCD prototype against model plant mismatches. In fact, the linear MPC has been integrated in the previous season on the vehicle has been exploit for the controlling of the sole vehicle lateral dynamics for the achievement of path tracking goal.

However, HIL simulation for the MPC integration has pointed out a delay into the actuation of the TV control, hence the two controllers are not perfectly synchronized with the real vehicle behaviour.

Thus, the focus of this thesis has finalized to use the predicted yaw rate state of the vehicle from a lateral MPC block, very similar to the one already integrated on the prototype, as yaw rate reference in substitution of the steady-state reference usually used in TV in literature. This strategy has demonstrated that the application of the TV design in thesis improves the vehicle performances, especially in the case of the presence of plant model mismatch. Hence, when the plant model presents slightly differences respect to the predictive model due to the presence of parameters estimation or linearization, the TV acts limiting the estimation inaccuracy of the MPC and performing a model following of the plant model to the MPC internal model. In particular, the mainly positive results obtained concern the reduction of the steering effort and the anticipation of the steering command, the reduction of the cross-track errors for achieving a better path-tracking, and the reduction of the deviations of between the vehicle states and the reference predicted states.

The promising effects are confirmed by the figures and tables presented in the previous chapter, proving that the solution proposed in this thesis can furtherly improve the overall performances of the autonomous prototype for the next Formula SAE seasons.

Future works

Regarding the future works, the first step is the integration in the prototype hardware of the controller proposed in this thesis which exploit the predicted yaw rate state from the MPC as reference for the TV control. Successively, the conduction of Hardware in the Loop (HIL) testing follows to have the real-time confirmation of the promising results obtained in the simulations developed with MATLAB/Simulink and VI-CRT.

Moreover, a further development can include also the design of a linear MPC which takes into account also the longitudinal dynamics of the vehicle in conjunction to the lateral one. A second MPC improvement can include also the study of non-linear approaches for a more accurate modelling of the real vehicle system. These enhancements in the MPC designing are particularly effective since would allow to achieve higher levels of reliability and consistency in the estimation of vehicle behaviour, limiting the errors due to the assumption of constant longitudinal vehicle speed and due to the linearization of the vehicle model. A consequent advantage is that the TV action will be totally focused on the increasing of the vehicle performances in cornering, stability and path tracking, instead of the overcoming of the eventual plant model mismatches.

In the end, different strategies can be analysed concerning the TV objectives, which can include the optimization of the electrical power consumption, the limitation of the longitudinal and lateral tire slipping and similar, to explore other solutions in favour of vehicle's stability and handling.

Bibliography

[1] L. De Novellis, A. Sorniotti, P. Gruber, and A. Pennycott, "Comparison of Feedback Control Techniques for Torque-Vectoring Control of Fully Electric Vehicles", *IEEE Transactions on vehicular technology*, vol. 63, no. 8, Oct. 2014

[2] A. Mangia, B. Lenzo, and E. Sabbioni, "An integrated torque-vectoring control framework for electric vehicles featuring multiple handling and energy-efficiency modes selectable by the driver", *Meccanica*, vol. 56, pp. 991-1010, May 2021, Available: https://doi.org/10.1007/s11012-021-01317-3.

[3] M. Asperti, M. Vignati, E. Sabbioni, "On Torque Vectoring Control: Review and Comparison of State-Of-The-Art Approaches", *Machines*, 2024, 12, 160. https://doi.org/10.3390/machines12030160.

[4] C. Chatzikonis, A. Sorniotti, P. Gruber, M. Bastin, "Torque-Vectoring Control for an Autonomous and Driverless Electric Racing Vehicle with Multiple Motors", *SAE Int. J. Veh. Dyn., Stab., and NVH 1(2):2017*, doi: 10.4271/2017-01-1597.

[5] J. Kang, Yi kyongsu, and H. Heo, "Control Allocation based Optima Torque Vectoring for 4WD electric Vehicle", SAE International, July 2020.

[6] S. Nekkah, J. Janus, M. Boxheimer, L. Ohnemus, S. Hirsch, B. Schimidt, Y. Liu, D. Borbély, F. Keck, K. Bachmann, L. Blezynski, "Autonomous Racing Software Stack of the KIT19d", Karlsruhe Institute of Technology, Karlsruhe, Germany, Oct. 2020.

[7] J. Kabzan, M. I. Valls, V. J.F. Reijgwart, H. F.C. Hendrikx, C. Ehmke, M. Prajapat, A. Buhler, N. Gosala, M. Gupta, R. Sivanesan, A. Dhall, E. Chisari, N. Karnchanachari, S. Brits, A. Liniger, J. Lygeros, R. Siegwart, "AMZ Driverless: The Full Autonomous Racing System", ETH Zurich, Zurich, Switzerland, May 2019.

[8] Y. Ren, L. Zheng, A. Khajepour, "Integrated model predictive and torque vectoring control for pat tracking of 4-wheel-driven autonomous vehicles", *IET Intelligent Transport Systems*, vol. 13, pp. 98-107, 2019, The Institution of Engineering and Technology 2018.

[9] SAE International. www.sae.org. https://www.sae.org./site/

[10] Society of Automotive Engineers (SAE International). https://golden.com/wiki/Society_of_Automotive_Engineers_(SAE_International)-R9Y6EJ4#References

[11] SAE International. *"Taxonomy and Definitions for Terms Related to Driving Automation Systems for On-Road Motor Vehicles", June 2018* https://www.sae.org/standards/content/j3016_201806

[12] National Highway Traffic Safety Administration. *"Automated Vehicle Safety"*. https://www.nhtsa.gov/vehicle-safety/automated-vehicles-safety

[13] *What is ADAS?* Published: 9 June 2023 [Online]. Available: https://www.ni.com/en/solutions/transportation/adas-and-autonomous-driving-testing/what-is-adas.html

[14] H.B. Pacejka, *"Tyre and Vehicle Dynamics"*, Oxford, UK: Butterworth-Heinemann, Second Edition, 2006.

[15] R. Rajamani, *"Vehicle Dynamics and Control"*, Springer, US, Second Edition, 2012, DOI 10.1007/978-1-4614-1433-9.

[16] A. Gimondi, M. Corno, S. M. Savaresi, "A Yaw Rate Based Stability Control for Under-Actuated Vehicles", IEEE Xplore.

[17] F. Borelli, A. Bemporad, M. Morari, "*Predictive Control for Linear and Hybrid Systems*", Cambridge University Press, UK, First Edition, 2017, p. 273

[18] P.Stano, U. Montanaro, D. Tavernini, M. Tufo, G. Fiengo, L. Novella, A. Sorniotti "Model predictive path tracking control for automated road vehicles: A review", ScienceDirect, Nov. 2022. Available Online: https://doi.org/10.1016/j.arcontrol.2022.11.001

[19] A. Di Rosio, "Design, Simulation and Testing of a linear MPC for lateral dynamic control of a Formula Student Driverless prototype". Polytechnic of Turin, Mechatronic Engineering Master's Degree, 2023

[20] Manca, Raffaele, et.al. "Optimal Torque-Vectoring Control Strategy for Energy Efficiency and Vehicle Dynamic Improvement of Battery Electric Vehicles with Multiple Motors", No. 2023-01-0563, 2023. SAE Technical Paper, 2023. DOI: 10.4271/2023-01-0563

[21] K. J. Åström, R. M. Murray, "*Feedback Systems*", Princeton University Press, US, Second Edition, 2020, Available Online: http://fbsbook.org.

[22] Castellanos Molina, Luis M., et al. “Predictive handling limits monitoring and agility improvement with torque vectoring on a rear in-wheel drive electric vehicle”, Vehicle System Dynamics (2023), 1-25.